Progress in Thermochemical Water Splitting with the Cu-Cl Cycle for Hydrogen Production

G. F. Naterer[1]*, S. Suppiah[2], M. A. Rosen[3], K. Gabriel[4], I. Dincer[5], O. Jianu[6], Z. Wang[7], E. B. Easton[8], B. M. Ikeda[9], G. Rizvi[10], I. Pioro[11], K. Pope[12], J. Mostaghimi[13], S. Lvov[14]

[1, 12] Memorial University of Newfoundland, St. John's, Newfoundland, Canada
[2] Canadian Nuclear Laboratories, Chalk River, Ontario, Canada
[3-6, 8-11] University of Ontario Institute of Technology (UOIT), Oshawa, Ontario, Canada
[7] Xiamen University, Xiamen City, Fujian Province, China
[13] University of Toronto, Toronto, Ontario, Canada
[14] Pennsylvania State University, University Park, Pennsylvania, U.S.

Abstract

This paper presents recent advances by an international team of five countries – Canada, U.S., China, Slovenia and Romania – on the development and scale-up of the copper chlorine (Cu-Cl) cycle for thermochemical hydrogen production using nuclear or solar energy. Electrochemical cell analysis and membrane characterization for the CuCl/HCl electrolysis process are presented. Constituent solubility in the ternary CuCl/HCl/H_2O system and XRD measurements are reported in regards to the $CuCl_2$ crystallization process. Materials corrosion in high temperature copper chloride salts and performance of coatings of reactor surface alloys are examined. Finally, system integration is examined, with respect to scale-up of unit operations, cascaded heat pumps for heat upgrading, and linkage of heat exchangers with solar and nuclear plants.

[1]* Corresponding Author: Professor and Dean, Faculty of Engineering and Applied Science, Memorial University of Newfoundland, St. John's, NL, A1B 3X5, Email: gnaterer@mun.ca; Phone: (709) 864-8864
[2] Manager, Hydrogen Isotopes Technology Branch, Canadian Nuclear Laboratories, Chalk River, Ontario, Canada, K0J 1J0
[3] Professor of Mechanical Engineering, UOIT, 2000 Simcoe Street North, Oshawa, Ontario, Canada, L1H 7K4
[4] Professor of Mechanical Engineering, UOIT, 2000 Simcoe Street North, Oshawa, Ontario, Canada, L1H 7K4
[5] Professor of Mechanical Engineering, UOIT, 2000 Simcoe Street North, Oshawa, Ontario, Canada, L1H 7K4
[6] Hydrogen Project Manager, UOIT, 2000 Simcoe Street North, Oshawa, Ontario, Canada, L1H 7K4
[7] Professor, College of Energy, Xiamen University, Xiamen City, Fujian Province, China, 361102
[8] Associate Professor of Chemistry, UOIT, 2000 Simcoe Street North, Oshawa, Ontario, Canada, L1H 7K4
[9] Associate Professor, Faculty of Energy Systems and Nuclear Science, UOIT, 2000 Simcoe Street North, Oshawa, Ontario, Canada, L1H 7K4
[10] Associate Professor of Mechanical Engineering, UOIT, 2000 Simcoe Street North, Oshawa, Ontario, Canada, L1H 7K4
[11] Professor, Faculty of Energy Systems and Nuclear Science, UOIT, 2000 Simcoe Street North, Oshawa, Ontario, Canada, L1H 7K4
[12] Assistant Professor of Mechanical Engineering, Memorial University of Newfoundland, St. John's, NL, A1B 3X5
[13] Professor of Mechanical Engineering, Director, Centre for Advanced Coatings Technologies, University of Toronto, Toronto, Ontario, Canada, M5S 3E5
[14] Professor of Energy and Mineral Engineering, Pennsylvania State University, 207 Hosler Building, University Park, PA 16802

1. Introduction

The copper-chlorine (Cu-Cl) cycle of thermochemical water splitting is a promising method of large-scale hydrogen production from nuclear, solar or other thermal energy sources [1, 2]. It offers significant advantages over other thermochemical cycles such as lower temperature operating requirements (below 550^{o}C). It consists of four main steps: 1) hydrolysis, 2) thermolysis, 3) electrolysis, and 4) water separation (e.g. crystallization) [3-5] – which together split water into hydrogen and oxygen through intermediate copper and chlorine compounds. Other thermochemical cycles have been identified in a Nuclear Hydrogen Initiative [6], including the sulfur-iodine [7], cerium-chlorine [8] and iron-chlorine [9] cycles. Funk [10] and Naterer et al. [11] presented a comprehensive review of hydrogen production by thermochemical water decomposition.

In the CuCl/HCl electrolysis step, oxidation of copper (I) chloride (CuCl) during an electrochemical reaction occurs in the presence of hydrochloric acid (HCl) to generate hydrogen. The Cu(I) ion is oxidized to Cu(II) at the anode, and the hydrogen ion is reduced at the cathode. This CuCl/HCl electrolysis process was first demonstrated for a long duration by Canadian Nuclear Laboratories (CNL) [12, 13]. A long duration of performance was demonstrated for 1,600 h of continuous operation with a cell voltage of approximately 0.7V at 45°C [3]. Significant developments in CuCl/HCl electrolysis have also been demonstrated experimentally at Pennsylvania State University [14] and the University of Ontario Institute of Technology [15]. Alternative membranes to mitigate the adverse effects of copper crossover have been reported [16] as well as Nafion-based and porous polyethylene (PPE) membranes to inhibit copper transport with HCl as a catholyte [17, 18]. It was shown that the current efficiency is more than 95% when the cell potential is stable at 0.7V, and the current density is 0.5A.cm^{-2} for a 36 h test using a Nafion-based membrane.

Early studies of the Cu-Cl cycle used spray drying processes to extract solid $CuCl_2$ from the aqueous solution exiting the electrochemical cell. However this was subsequently determined to be energy intensive, and led to undesirable vaporization of other compounds, so alternatives such as crystallization were explored.

Wang et al. [19] reported on the integration of electrolysis and hydrolysis steps using crystallization of $CuCl_2$ particles from the electrochemical cell. Leray [20] and Abdel [21] have previously examined the growth kinetics of hydrated copper (II) chloride ($CuCl_2 \bullet n_h H_2O$, where n is the number of hydrated water molecules) and recovery of cupric chloride from spent solutions. Crystallization of $CuCl_2$ is normally less energy intensive than spray drying because ambient air and cooling water can be sufficient for cooling the solution to ambient temperature.

Copper (II) chloride is the oxidation product of copper (I) chloride, hence copper (II) and copper (I) chlorides coexist in the aqueous solution of HCl. The solubility of copper (I) chloride (CuCl) in aqueous hydrochloric acid (HCl) at different molarities and temperatures [22-25] affects the crystallization process. The solubility of solid CuCl in aqueous HCl is much larger than in water [25]. The crystal sizes of chloro complexes and conversion rates from CuCl to $CuCl_2$ have been reported by O'Connor et al. [26]. Experiments were performed by Fritz [27] to determine the solubility of copper (I) chloride in various aqueous chlorides and their associated equilibrium constants of formation. It was found that a set of viral parameters representing the activity coefficients of the ions formed in dissolution. These past studies found that the solubility of CuCl is increased by the presence of a relatively low concentration of HCl compared to the solubility in water.

The hydrolysis reaction is an endothermic non-catalytic gas-solid reaction between 350 and 400^oC where $CuCl_2$ particles from the crystallization process are reacted with superheated steam to produce copper oxychloride solid ($CuOCuCl_2$, often denoted as Cu_2OCl_2) and hydrochloric gas (HCl). Extensive experimental studies [28, 29] were conducted at the Argonne National Laboratory (ANL) with a spray reactor to determine the mass flow rate of steam required to produce Cu_2OCl_2 using a mixture of argon/steam to supply heat to the reactor. Results indicated that 100% yields of Cu_2OCl_2 could be achieved with an ultrasonic nozzle to inject the reactants into the reactor at about 375^oC. Excess steam required for the heat supply reduces the overall cycle efficiency of the system. Pope et al. [30] examined the use of nitrogen to reduce the steam requirement of the hydrolysis reaction in a fluidized bed reactor. Equilibrium conversion rates, thermophysical properties

of compounds, and a gas film layer around the solid $CuCl_2$ particles are significant factors that influence the hydrolysis reaction [31, 32].

Materials of construction are major issues in the Cu-Cl cycle development. Limited data exists in past literature on the corrosion resistance of materials in molten CuCl. The most suitable materials for high temperature and corrosive environments are ceramics, refractory metals, molybdenum and nickel based alloys, graphite based materials, and Hastelloy C. Xie et al. [33] examined the corrosion of carbide/nitride materials in 2.5 mol/L HCl solutions at elevated temperatures. Wu et al. [34] tested mullite specimens in a 10 wt.% NaOH solution at 105 °C, assessed the formation of mullite, and examined a sol-gel coating to improve corrosion resistance. Sure et al. [35] reported the performance of partially stabilized zirconia (PSZ) with graphite coatings at 600°C and found that PSZ corroded by adding oxygen to the surface. Experimental findings of the corrosion of graphite in molten LiCl, and graphite powder mixed with 46 wt.% LiCl that were melted to change the molten salt structure, were reported by Kamali and Fray [36]. The corrosion behavior of Hastelloy C276, C-22 and N was examined at 250 and 500°C in dry molten salt with a composition of 13.4 mol% NaCl, 33.7 mol% KCl and 52.9 mol% ZnCl2 (Vignarooban et al. [37]). Sellers et al. [38] investigated the corrosion rates of Hastelloy N and Steel 316 immersed for 100 h at 850°C in a molten salt consisting of 46.5 mol% LiF, 11.5 mol% NaF and 42 mol% KF. Siantar [39] conducted experiments to examine the performance of metallic and ceramic coatings on a base metal exposed to molten CuCl at 500°C.

A number of other related studies associated with the Cu-Cl cycle were conducted by the international team including exergo-economics using exergy-cost-energy-mass (EXCEM) analysis [40, 41], life cycle analysis [42], environmental impacts [43], applications in the transportation sector [44], and integrated systems with geothermal energy [45], solar energy [46, 47] and desalination plants [48]. The team is collaborating on the development of enabling technologies for the Cu-Cl cycle, through the Generation IV International Forum (GIF). This paper describes the progress of development of these enabling technologies, particularly focusing on recent advances presented at workshops in 2015 and 2016 in Oshawa, Ontario [49, 50], involving CuCl/HCl

electrolysis, crystallization, constituent solubilities in ternary mixtures, materials corrosion, and scale-up of unit operations.

2. Thermochemical Copper Chlorine (Cu-Cl) Cycle

The 4-step Cu-Cl cycle consists of a sequence of four main steps: 1) hydrolysis (water splitting), 2) thermolysis (oxygen production), 3) electrolysis (hydrogen production), and 4) water separation by crystallization or spray drying.

- Step 1: Hydrolysis (endothermic)

  $2CuCl_2 \bullet n_h H_2O(s) + H_2O(g) = CuOCuCl_2(s) + 2HCl(g) + n_h H_2O(g)$, n_h is 0~4 at 400°C (1)

- Step 2: Thermolysis (endothermic)

  $CuOCuCl_2(s) = 2CuCl(molten) + 0.5O_2\ (g)$, at 530°C (2)

- Step 3: Electrolysis

  $2CuCl(aq) + 2HCl(aq) = 2CuCl_2(aq) + H_2(g)$, in aqueous solution of HCl, at 90°C (3)

- Step 4: Water separation (endothermic)

  $CuCl_2(aq) + n_f H_2O(l) = CuCl_2 \bullet n_h H_2O(s) + (n_f - n_h)H_2O$

  $n_f > 7.5$, n_h = 0~4, at 30~80°C (crystallization) or 100~260°C (spray drying) (4)

Figure 1 illustrates a schematic of the thermochemical cycle. This water splitting process begins when water enters the thermochemical plant, recovers heat, forms steam, enters the hydrolysis reactor, and then reacts with copper (II) chloride (solid) to form copper oxychloride (solid) and hydrochloric gas. The HCl/H_2O gas leaves the hydrolysis reactor, condenses in an aqueous solution, and enters the electrolysis reactor. The exiting copper oxychloride particles are transported to the thermolysis reactor and decomposed to produce oxygen gas and molten CuCl. Molten CuCl leaves the oxygen reactor, enters an intermediate heat exchanger which recovers heat, thus changing phase to solid, and then moves to the electrolyzer for electrolysis of the aqueous HCl/CuCl mixture. Solid CuCl particles are dissolved in aqueous HCl before reaching the

electrolysis cell. For efficient operation of the Cu-Cl cycle, it is important to efficiently design the intermediate heat exchangers to recover as much heat as possible from each of the hot product streams.

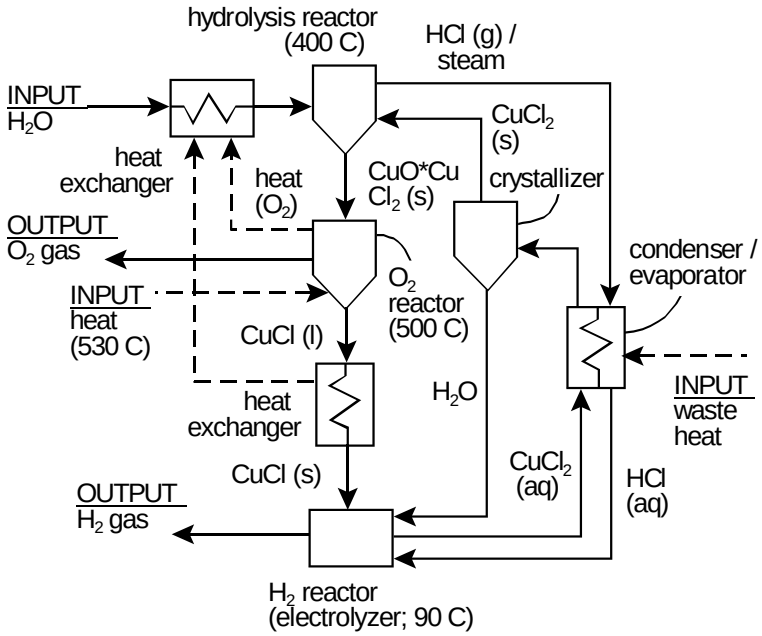

Figure 1: Schematic of a thermochemical copper-chlorine cycle [2]

3. CuCl/HCl Electrolysis

3.1 Electrochemical Cell Analysis

Analysis of the electrochemical kinetic equations has been performed to predict the equilibrium state limitations on the anode side of the electrolyzer [49]. Concentrations were determined for anolyte species and sensitivity analyses of equilibrium states were conducted at varying temperatures. With reference to Fig. 2, five overall reactions occur in the electrochemical cell.

- Dissociation: $\mathrm{CuCl(s)} \Leftrightarrow \mathrm{Cu^{+}(aq) + Cl^{-}(aq)}$ (5)
- Dissociation: $\mathrm{HCl(l)} \Leftrightarrow \mathrm{H^{+}(aq) + Cl^{-}(aq)}$ (6)
- Oxidation: $\mathrm{Cu^{+}(aq)} \Leftrightarrow \mathrm{Cu^{+2}(aq) + e`}$ (7)
- Reduction: $\mathrm{Cu^{+2}(aq) + 2Cl^{-}} \Leftrightarrow \mathrm{CuCl_2(aq)}$ (8)
- Reduction: $\mathrm{H^{+}(aq) + e} \Leftrightarrow \mathrm{0.5H_2(aq)}$ (9)

Reactions (5) and (6) occur in the CuCl-HCl-H_2O region of the anolyte tank where CuCl and HCl dissociate into their ions, respectively. Depending on concentrations, CuCl(s) dissociation might be incomplete after passing the solubility limit. The solution pumped to the anode side of the cell has aqueous ions. Equations (7) and (8) represent oxidation of Cu(I) species on the anode surface and reduction of Cu^{2+} in the anolyte bulk solution. As reduction in Eq. (9) proceeds, hydrogen gas bubbles flow up toward the storage tank.

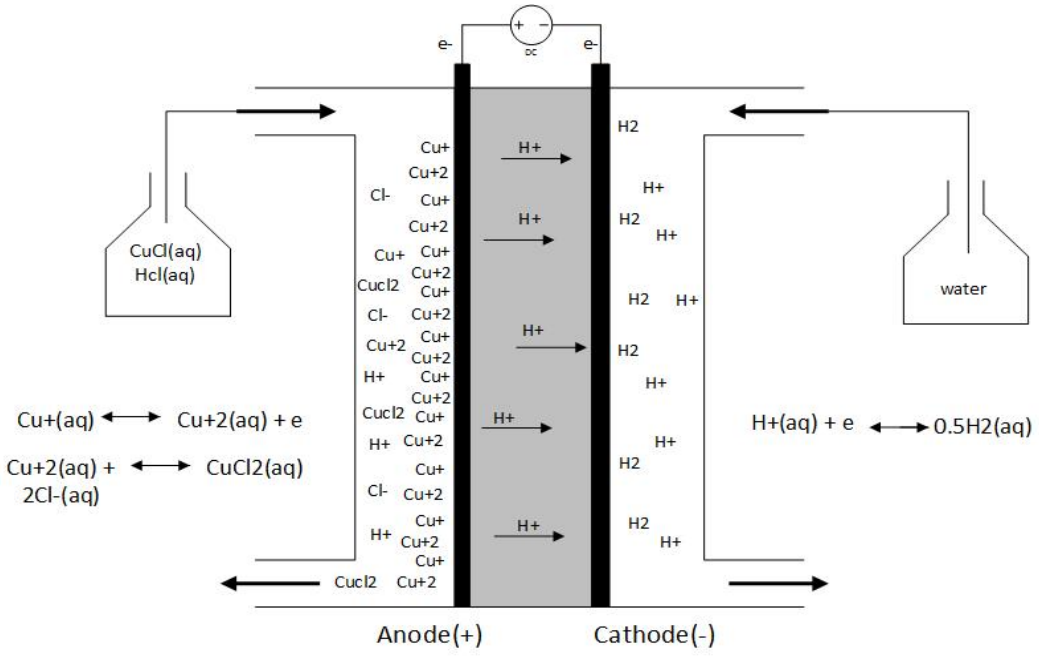

Figure 2: Schematic of the CuCl/HCl electrolyzer

The anode half-cell was examined to find the equilibrium constant for Eq. (7) on the electrode and determine if the standard potential satisfies the equilibrium condition of Eq. (8). In the analysis, a copper ion loses an electron on the anode surface, free electrons out of the equilibrium barrier pass through the external circuit and Cu^{2+} is reduced by free Cl^{-} ions to reach equilibrium. Also, hydrogen ions are carried by water molecules as hydronium to the cathode side for hydrogen production. The equilibrium system is consistent for all three reactions, i.e., reactions (7) to (9).

An electrochemical model was developed for the electrolyzer cell and focused on the anode side to study the reaction kinetics [49]. Thermodynamic temperature-dependent properties for aqueous substances

were used to relate thermodynamics of the process to electrochemistry through the Gibbs free energy change of reactions. Furthermore, investigations were conducted to determine the variation of the standard potential of the anodic redox reaction with respect to temperature and ionic concentration changes.

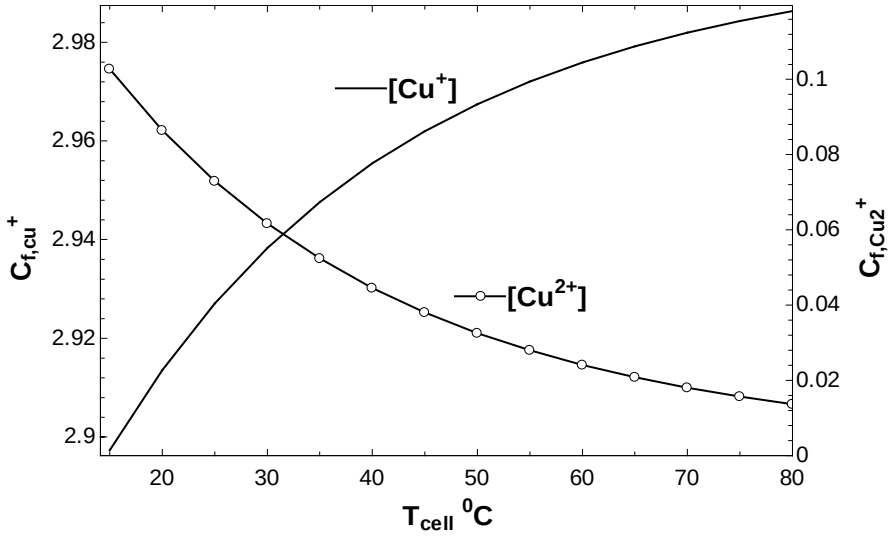

Figure 3: Effects of temperature on equilibrium concentrations of anodic reaction ions

Sample results from the analysis are shown in Fig. 3. As the temperature rises, the equilibrium state concentration of Cu^{2+} decreases. It was found that high anolyte temperature does not permit the anodic redox reaction to proceed to the products side, so electron charges cannot readily flow through the external circuit in such conditions. An increase of the applied potential on the anode results in a redox reaction moving towards the product side. This effect is weaker at higher temperatures. Also, in order to establish equilibrium at the same time for the anodic redox reaction and also $CuCl_2$ formation at the same working conditions, the applied potential for the redox reaction cannot be lower than 0.19 V (at 25ºC) while the standard redox potential for this temperature is 0.16 V.

3.2 Electrolysis Membrane Characterization

The electrochemical cell employs a membrane electrode assembly (MEA) that utilizes a proton exchange membrane (PEM). The most widely used PEM, Nafion, is permeable to cations and neutral species. Thus Cu can permeate the membrane and enter the cathode where it is readily deposited on Pt catalytic sites. This drastically reduces cathode efficiency as well as the whole cell. Recent studies [49]

examined several alternative membranes, including Nafion/polypyrrole and Nafion/polyaniline composite membranes. Ex situ permeation experiments were performed along with impedance spectroscopy to investigate the rate of copper crossover and conductivity of the composite membranes, respectively.

The ion-exchange capacity (IEC) of the membranes was measured by titration. Since IEC represents the exchangeable cationic species such as protons (H^+) which interact with the sulphonic groups, the IEC results were used to determine the relative quantity of polyaniline (PANI) in the composite membranes. As the membranes with PANI were modified, the IEC values noticeably decreased to 0.5 meq/g, as presented in Table 1. This reduction reflects the amount of PANI interacting with the sulfonic groups in the membranes. As expected, when PANI chains replaced the H^+ and interact with the sulfonic groups, the IEC value decreased as less protons were available for replacement. Both PANI composite membranes of N115 and N117 showed nearly the same reduction trend of the IEC values. Furthermore, changing the concentration of aniline from 0.2 M to 0.5 M had very little effect on the value of IEC. In addition, comparing the values of IEC of the PANI composite membranes with the Ppy composite membranes, it was found that Ppy composite membranes have lower IEC values, indicating a larger quantity of Ppy in the membrane.

membrane	% Water uptake	IEC(meq/g)	Conductivity S/cm	Permeability cm^2/s	Selectivity $S.s/cm^3$
N115	26.8	0.854	9.78E-02	6.86E-07	1.43E+05
N115-0.2M PANI $FeCl_3$ 24 c	13.7	0.579	2.35E-02	4.20E-07	5.60E+04
N115-0.5M PANI $FeCl_3$ 24 c	17.1	0.543	2.37E-02	3.76E-07	6.29E+04
N117	31.4	0.847	1.19E-01	1.05E-06	1.13E+05
N117-0.2M PANI $FeCl_3$ 24 c	20.4	0.573	3.53E-02	4.94E-07	7.14E+04
N117-0.5M PANI $FeCl_3$ 24 c	20.1	0.560	2.77E-02	4.78E-07	5.80E+04

Table 1: Physical properties of PANI composite membranes and pristine Nafions

Figure 4 illustrates full cell H_2 cyclic voltammograms (CV) for a pure Nafion N115 membrane and other composite membranes after 3 working days (abbreviated d). Measurements were taken at a sweep rate of 50 mV s^{-1} at 25°C with 2.0 M HCl flowing in the left side of the electrochemical cell at 60 mL/min and H_2 flowing in the right side at 25 mL/ min. This experiment was used to detect any copper species deposited from the copper crossover during regular cell operation. The first day of the CV measurement, for all

membranes, did not show any traces of copper deposition. Previously prepared Ppy composite membranes were used for comparison.

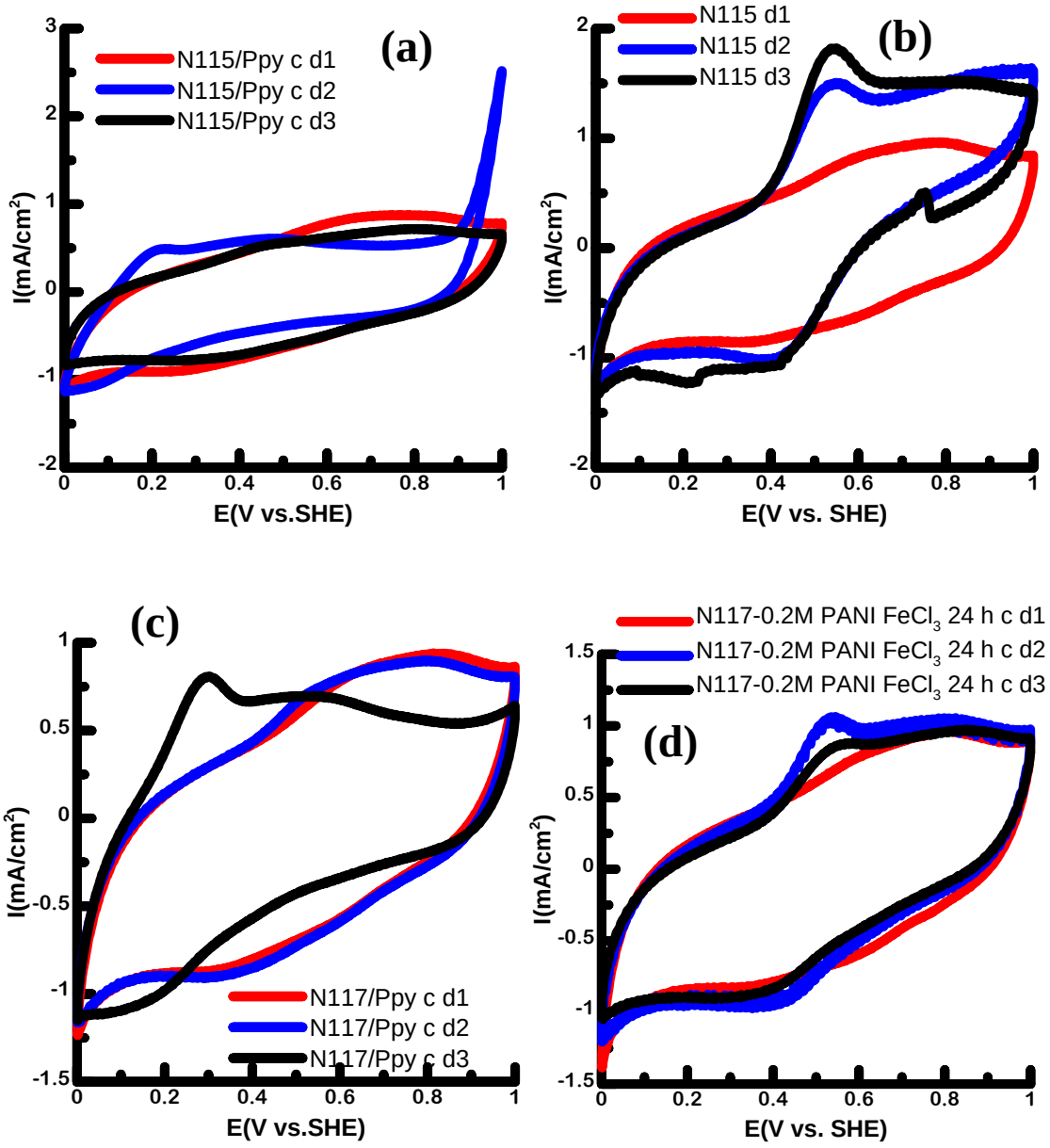

Figure 4: Full cell H_2 from cyclic voltammograms (CV) for pure Nafion N115 membrane and other composite membranes: (a) N115/Ppy c (b) N115 (c) N117/Ppy c (d) N117-0.2M PANI $FeCl_3$ 24 h

The CV measurement of N115/Ppy c membranes for the 3 days did not display any oxidation or reduction peaks at 0.4-0.5 V as can be seen in Fig. 4 (a), which could be a positive sign of absence of any copper crossover. Figure 4 (b) illustrates the CV measurements of the N115 pristine membrane. It clearly shows the oxidation and reduction peaks on the second and third testing days, whereas these peaks were

absent on the first day. These peaks are attributed to the oxidation and reduction of copper accumulated as a result of crossover. The CV measurements obtained for N117/Ppy c and N1170.2M PANI $FeCl_3$ 24 h c are shown in Figs. 4 (c) and (d), respectively. The CV measurements of N117/Ppy c membrane did not show any oxidation or reduction peaks for the first and second day. An oxidation peak appeared at 0.3 V without any clear reduction peak. This peak does not likely relate to copper crossover as it does not match the 0.4-0.5 value. The CV measurements of N117-0.2M PANI $FeCl_3$ 24 h c membrane showed small oxidation reduction peaks as illustrated in Fig. 4 (d). These small peaks indicate that there was some copper deposition. The experiments found that N115/Ppy c performance was the best amongst the tested membranes.

4. $CuCl_2$ Crystallization

4.1 XRD Measurements of $CuCl_2$ Crystallization

Crystallization is an effective method to recover solids from solution, due to its relatively low energy utilization and cost compared to other methods such as spray drying. Several experiments have been conducted to determine the range of concentrations from which crystallization occurs in the aqueous $CuCl_2$ stream exiting the electrochemical cell. If the initial concentration exceeds the upper solubility limit, the solution will be saturated and become a paste-like substance without forming crystals. Conversely, if the initial concentrations fall below the lower bound, the solution will remain liquid upon cooling. The experimental apparatus is illustrated in Fig. 5. Crystallization was not observed in the studies for HCl concentrations below 3 mol/L and above 9 mol/L. To analyze the composition of the recovered solids, X-ray diffraction (XRD) was employed. Also, $CuCl_2$ samples were analyzed using thermogravimateric analysis (TGA) to determine thermochemical properties such as melting and decomposition temperatures. The stationary point on the TGA curve was determined to be 442°C, which is below the normal melting temperature of $CuCl_2$.

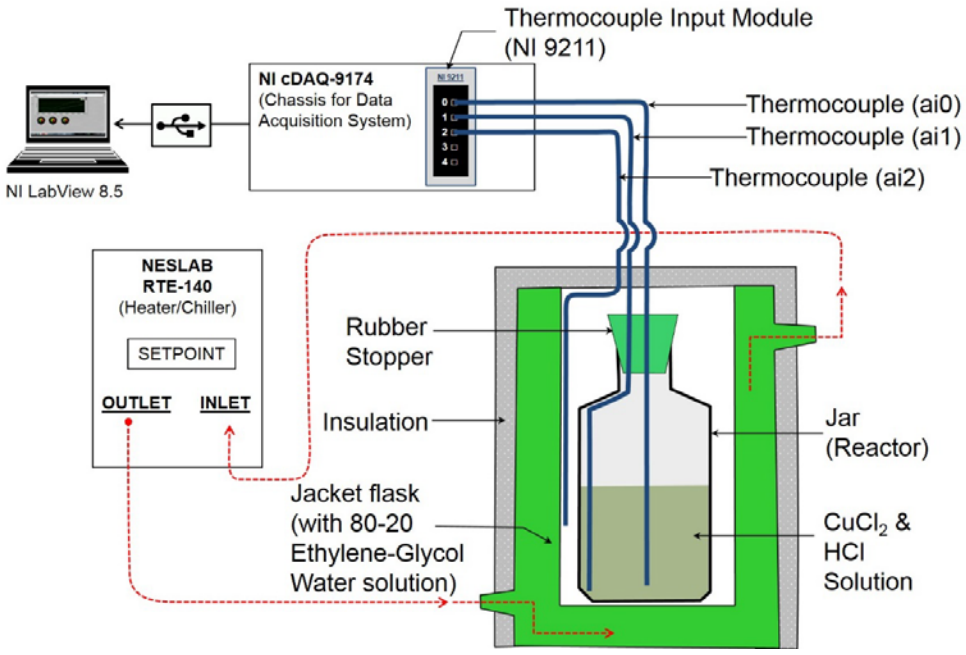

Figure 5: Experimental setup for crystallization measurements at varying temperatures

It was observed that most crystallization occurs within minutes of the formation of the first crystal from which growth propagates. Crystallization will take longer if no crystallizing agent is added to the mixture. For most samples tested at molarities lower than 5 mol/L, the crystallization only starts after the temperature of the system falls below 30^{o}C. It was also found that a colder solution yields larger particles. Figure 6 shows the crystallized $CuCl_2$ before filtering out the clear solution. Compared to the crystal size of other salts, $CuCl_2$ crystals are relatively small yet still observable without specialized equipment.

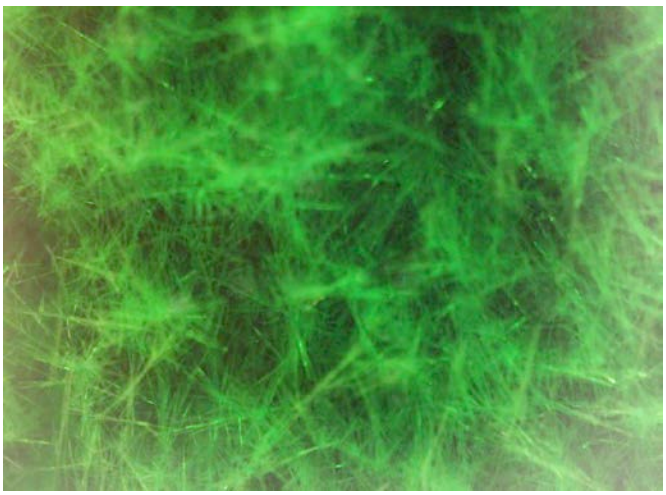

Figure 6: Configuration of crystalline solid (green dendrites) at temperatures below room temperature

X-ray diffraction is a measurement technique in which atomic planes of a crystal cause the incident beam of x-rays to interfere with each other as they leave the crystal. The spacing between layers of atoms is measured and the orientation of a single crystal is found. Once the orientation is determined, the crystal structure size, shape and internal stress of crystalline regions of the material can be found. A measured XRD pattern for $CuCl_2$ crystallization is illustrated in Fig. 7. The plot indicates that the crystals formed through the crystallization process were $CuCl_2$ dihydrate, i.e., $CuCl_2 \cdot 2H_2O$. However, an impurity (botallackite) was also detected. From the experimental studies, it was observed that anhydrous copper (II) chloride does not crystallize. Also, crystallization did not occur at concentrations above 9 mol/L. HCl acts as a "crystallizing agent", causing near-instantaneous crystallization when it is added to the aqueous $CuCl_2$ solution. Crystallization occurred consistently when the solution temperature fell below the saturation temperature.

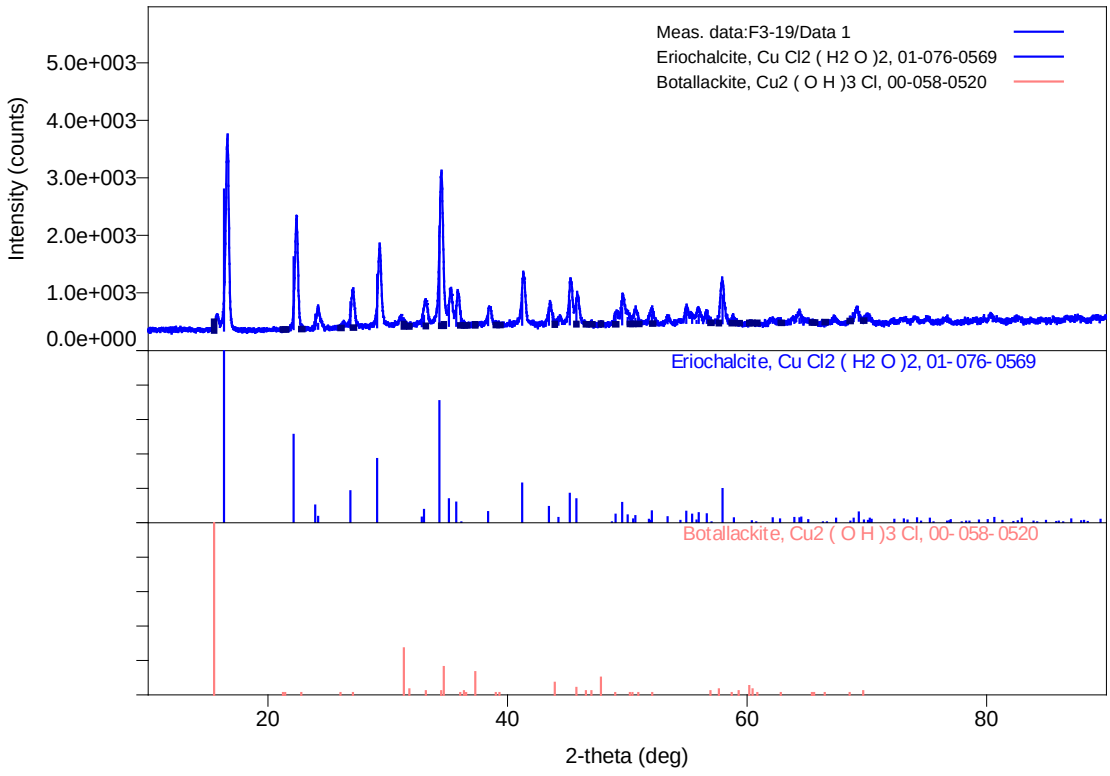

Figure 7: Experimental results of XRD measurements

4.2 Constituent Solubility in Ternary HCl/HCl/H_2O System

A ternary system of copper (I) chloride (CuCl), hydrochloric acid (HCl) and water exists in the electrochemical cell. Solubility data of the constituents is important to understand the transport processes and thermodynamic equilibrium in terms of the concentration of the copper (I) ions. The dissolution of CuCl occurs in the electrochemical cell where CuCl solute dissolves in the solvent (aqueous HCl) to form a solution by disintegrating the solute's structure into separate ions of Cu^{+} and Cl^{-}. The dissolution kinetics and maximum extent are determined by the solubility, which indicates the thermodynamic limit.

An experimental apparatus was designed and built to melt CuCl powder and create solid CuCl blocks and pellets to examine their dissolution kinetics in aqueous HCl solutions. To avoid CuCl oxidation due to the presence of oxygen, melting was performed in an atmosphere of high purity (99%) nitrogen. Figure 1 shows the apparatus used to melt CuCl powder. Once the powder in the test tubes was melted, the apparatus was placed in the purged glove box and the melted CuCl was solidified. The extracted CuCl blocks were weighed and stored in airtight containers purged with high purity nitrogen.

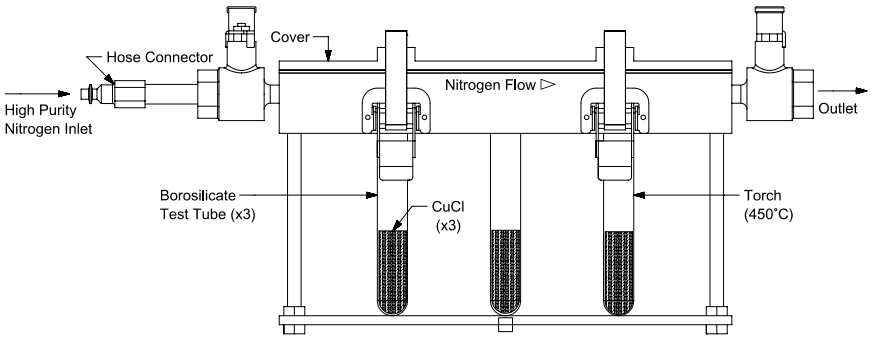

Figure 8: Apparatus to melt powder CuCl and create solid CuCl

The solubility of CuCl(s) in HCl(aq) with different concentrations at varying temperatures was then investigated. Four different HCl(aq) solutions were prepared (3M, 6M, 9M and 12M) and the solubility was determined at two different temperatures (25ºC and 40^{oC}). Solid CuCl blocks were dropped in a 100 ml HCl(aq) solution and allowed to dissolved until saturation was achieved. The four different concentrations of HCl (i.e., 3M, 6M, 9M and 12M) corresponded to an HCl to water ratio of 0.053, 0.132, 0.265 and 0.568, respectively. Figure 9 presents a comparison between the measured data from previous studies. The

measured data is consistent with previously reported data at lower concentrations (3M and 6M). Also, the measured data at higher concentrations appears to follow a similar trend of the curve obtained at lower concentrations.

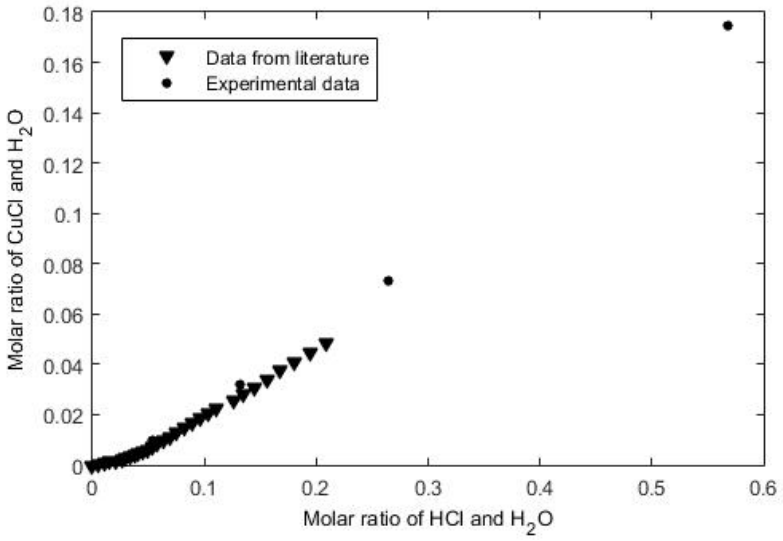

Fig. 9: Measured solubility of the ternary CuCl-HCl-H_2O system at 25^oC

4.3 Metastability of $CuCl_2$ in H_2O-HCl

The solid-liquid phase change temperature is dependent on the direction of temperature change (i.e., heating or cooling). During a heating process, the dissolving temperature increases whereas during cooling, the precipitation temperature decreases. The difference between these two temperatures is the Metastable Zone Width (MSZW). Precipitation occurs at a lower temperature thereby reducing the energy requirements of the phase change process. This process is a form of hysteresis.

Dissolution occurs at a temperature of T_d and precipitation occurs at T_{met}, therefore, MSZW = $T_d - T_{met}$. Recent studies [50] investigated the MSZW for ternary solutions of water (H_2O), hydrogen chloride (HCl), and copper (II) chloride ($CuCl_2$). The study examined the effects of cooling rate and HCl concentration on MSZW, as well as the effect of HCl concentration and initial temperature on K_{sp} (solubility product constant).

In the experiments, a heated solution of known molarity was prepared with a concentration below saturation. The unsaturated solution was cooled at a controlled rate until a crystal appeared. The temperatures were recorded and the solution was then heated until the crystal re-dissolves. Again the temperature was recorded and the difference in temperatures is the MSZW.

The value of K_{sp} was calculated in terms of Gibbs free energy. A plot of ln(MSZW) and ln(cooling rate) was found to be nearly linear. Most data points were within $\pm 1\sigma$ of the Wt. Avg. All points lie within $\pm 2\sigma$ of the Wt. Avg. The cooling rate was correlated with the MSZW and nucleation rate constant, K_N,

$$\ln(\text{Cooling Rate}) = m \times \ln(\text{MSZW}) + \ln(K_N) \quad (10)$$

where m is the nucleation order (slope) that characterizes how easily the solution nucleates (a mode of crystal formation) and K_N represents the nucleation rate constant ($\ln(K_N)$ corresponds to the y-intercept). Table 1 summarizes the resulting correlations at varying HCl concentrations.

HCl Concentration [M]	**m**	**y-int**	**k_N**	**Number of Data Points**
6	0.621	-6.16	2.11×10^{-3}	4
8	0.998	-6.06	2.34×10^{-3}	4
10	0.362	-5.59	3.73×10^{-3}	6
Mean	0.660	-5.94	2.64×10^{-3}	2.73×10^{-3}
Wt. Avg	0.618	-5.89	2.77×10^{-3}	2.87×10^{-3}

Table 2: Nucleation order and nucleation rate constants for several HCl concentrations

As illustrated in Fig. 10, MSZW decreases with HCl concentration and increases with cooling rate. The results also demonstrate that K_{sp} increases with temperature and decreases with HCl concentration. These trends are important for reducing the energy requirements associated with the crystallization process as more precise data on the precipitation temperature can lower the energy input. A larger MSZW is preferred since it lowers the crystallization (precipitation) temperature, thus reducing energy input requirements to the Cu-Cl cycle.

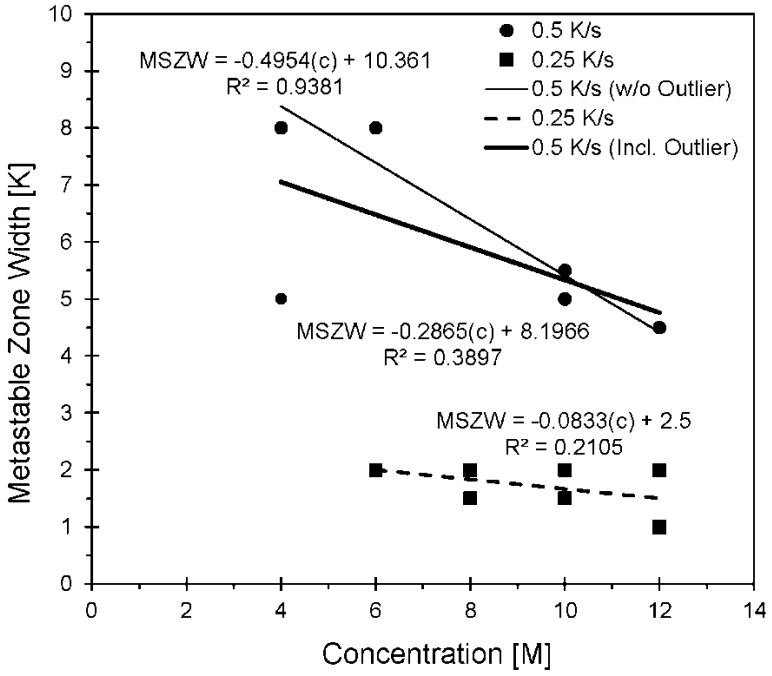

Figure 10: Effect of cooling rate on MSZW

5. Materials Corrosion

5.1 Material Corrosion in Molten Copper Chloride

An experimental apparatus was designed and built at UOIT to examine the corrosion resistance of various metal alloys to high temperature copper chloride salts. A schematic of the apparatus is shown in Fig. 1. CuCl powder was placed in an alumina crucible and melted in a heating mantle with a maximum temperature of 600°C. The alumina crucible was used to avoid reactions between the crucible and molten salt. To ensure safety, the height of the crucible and inside diameter of the heating mantle was chosen so that tipping of the crucible inside the mantle and spilling of the molten salt are prevented. To ensure the environment is free of oxygen, the system is purged with high purity nitrogen prior and during experimentation. Several type K thermocouples connected to a temperature controller are installed to measure the molten salt temperature and temperatures of the atmosphere outside the crucible. To prevent damage to the thermocouples in the molten salt, a thermal well consisting of a copper pipe is used. The copper does not react with the molten salt since the environment is free of oxygen. A standard 3-electrode arrangement is used to determine the corrosion behaviour.

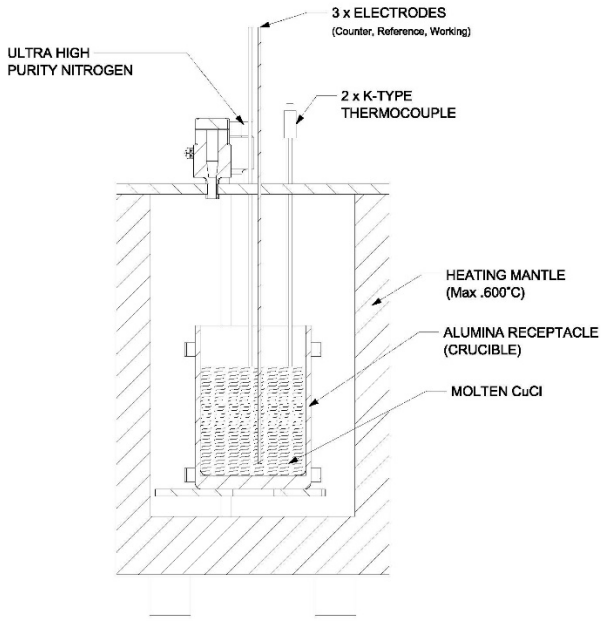

Figure 11: Experimental apparatus for corrosion resistance to molten CuCl

Corrosion reactions involve the transfer of electrons and ions between the material and the solution. The rate of electron transfer is an electric current that depends on the potential difference between the metal and solution. The potential of the working electrode (corrosion sample) in the test solution under study was measured against a reference electrode with a voltmeter. A fixed current is applied from a constant-current power source connected to the working electrode and a counter electrode. The change in potential at the working electrode caused by the impressed current forcing the oxidation reaction is then measured against the reference electrode.

A review of past studies suggested that nickel chrome alloys would be the best candidates for the corrosive molten CuCl environment. These alloys have performed well in high temperature and highly corrosive environments, as well as chloride rich environments. The alloys tested in the corrosion experiments were: Inconel 625, Inconel 825, Inconel 686, Inconel Alloy 22, Hastelloy N, and Stainless Steel 316.

Samples were exposed to molten CuCl at 450°C at various time intervals (2, 4, 8, 16, and 32 h) to determine the corrosion rate. All of the samples showed an impact of corrosion. All samples gained weight as a result of oxide phase formations, e.g., Cr_2O_3, Fe_2O_3, NiO. Also, all samples changed color as a result of the formation of an oxide layer. Many different colors were observed on the materials surface, which is indicative

of different thicknesses of oxide layers. The extent and rate of corrosion were determined by transient changes in weight. A weight gain on the samples was indicative of a layer of an adherent corrosion product layer. Also, X-ray diffraction was used to determine the presence of crystalline oxide phases. The surface structure was identified by scanning electron microscope (SEM) imaging.

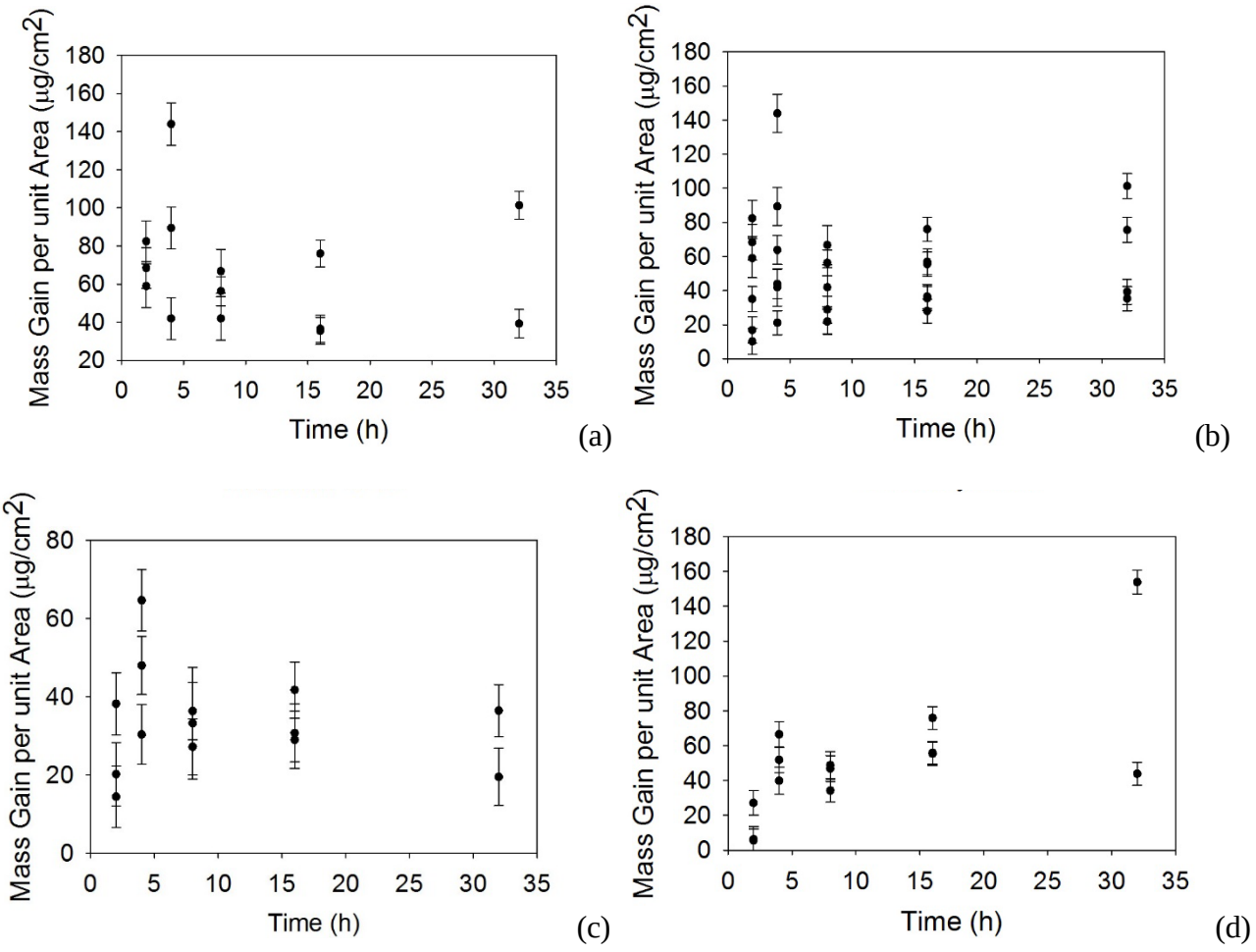

Figure 12: Mass gain per unit area for (a) Hastelloy N, (b) Inconel 22, (c) Inconel 625, and (d) Inconel 825

Figure 12 illustrates the results of mass gain per unit area for several alloys over time. Hastelloy was developed at Oak Ridge Laboratories for use in a liquid fluoride thorium reactor. It is a nickel alloy with high molybdenum content to prevent corrosion at high temperatures. Inconel 22 is a nickel and high chromium alloy (22 wt%) used primary in chloride and fluoride environments. It exhibits corrosion resistance in cupric salt environments. Inconel 625 is typically used in high chloride environments, as well as high temperature air environments due to its high molybdenum and chrome content. Finally, Inconel 825 is a nickel-chrome alloy

with an addition of titanium. Other alloys tested in the experiments include: Inconel 686 (nickel – chromium alloy) and Stainless 316 Iron alloy with an addition of chrome and molybdenum to aid in corrosion resistance.

Yellow crystallized solid formed at the top of the reactor. XRD results indicated that the crystal was copper (II) chloride dihydrate. As the top of the reactor is located outside of the furnace, a low temperature may have likely caused $CuCl_2$ to condense. No preferential deposition near the samples suggested that the environment was constant around the experimental region. The corrosion rates are low as very small weight changes were recorded over the test periods. The samples were exposed to the experiment conditions for long periods of time. Samples were analyzed by XRD and SEM imaging to determine the type of corrosion product found and surface characteristics.

5.2 Corrosion Resistant Coatings

5.2.1 Types of Coatings

Recent studies [50] reported the corrosion resistance of several metal alloys with various coatings in molten CuCl at 500°C. A variety of molten salts are used in industries having a wide range of possible chemical reactions with metallic surfaces. Molten salts mostly involve a mixture of carbonates, nitrates or alkaline metals or halides of the alkaline-earth and these usually have solubility for oxides of the other metals. The produced oxides do not form a protective coating and are consequently moved into the solution of molten salts and corrosion steadily progresses. In some cases adsorption of components of the salt mixture into the alloy can occur with adverse results.

Medium carbon steel was selected as the base metal in the corrosion experiments. After a series of immersion tests, the materials were evaluated with ex-situ surface analyses. The surface conditions, including film structure, elemental composition, and resistivity of the materials were examined and compared. Several combinations of coated specimens were evaluated: bare metal for oxidation tests, metal coated with Diamalloy 4006 as a metallic coating, metal coated with YSZ as a ceramic coating, metal coated with YSZ, and Diamalloy. Table 3 presents all samples evaluated in the immersion tests.

Coating	Sample	Abbreviation

0	Bare (uncoated) medium carbon steel - 1045	Mild
1	Medium carbon steel (1045) coated with YSZ coating	YSZ
2	Medium carbon steel (1045) coated with Diamalloy 4006 and YSZ coatings	Dia+YSZ

Table 3: List of sample coatings

The Ni based amorphous alloy Diamalloy 4006 (Ni 20Cr10W9Mo 4Cu 1C 1B 1Fe) coatings contain glassy (amorphous / microcrystalline) phases. There is microstructural homogeneity due to the absence of grain structures and microstructural features such as grain boundaries, micro segregation, and dislocations. YSZ (Zirconia, ZrO_2 8%Y_2O_3) coatings exhibit excellent scuff resistance, high temperature hardness, excellent thermal shock properties and resistance to sulfidation, chlorinization and sodium hot corrosion.

5.2.2 Experimental Apparatus

The immersion apparatus consists of an immersion test vessel (ITV), condenser vessel, scrubber vessel, and heating and control systems (see Fig. 13). The ITV consists of the body and lid that were made of fused quartz. The ITV lid has three insertion stems which are used for different functions: the first stem is used for a K-Type thermocouple to monitor the working temperature inside the ITV. Another stem is used for exhausting the hot gases through the connecting pipe to the condenser and the scrubber, and the third stem is for deaerating the atmospheric air by injecting inert gas (N_2) before and during operation. The pressure relief valve and specimen handling device are also connected to the third stem.

Figure 13: Experimental apparatus for coatings evaluation

The condenser is used to cool the exhaust gas of the ITV before exhausting it to the scrubber and then releasing to the environment by a fume hood. The function of the scrubber is to neutralize the exhaust gas before releasing it to the fume hood. The solution inside the scrubber is a mixture of water (4.5L) and saturated sodium bicarbonate ($NaHCO_3$) (390g). A heating mantle is used to produce molten CuCl. The temperature is adjusted by a PID controller and a thermal cut-off system to prevent excessive heating for safe operation.

Evaluation of samples is possible by visual examinations, weight changes, EIS tests, and SEM/EDX tests. Immersion tests were conducted according to ASTM procedure ASTM-G-31-72 – Standard Practice for Laboratory Immersion Corrosion Testing for Metals (ASTM 1998). The sealing mechanism is evaluated by examining oxidation of a bare metal.

Each sample was examined visually before and after the immersion test for CuCl attack (localized-uniformly). A color change can help distinguish the deposited materials. The sample was also evaluated by a shape change if it corroded severely or deposits remained on the sample surface to demonstrate the quantity/form of corrosion. Some pits were identified by visual examination or otherwise pits were deep enough to characterize their depth by optical means. Weight change measurements were made on mild steel blanks to determine the weight change before and after the immersion test in which samples were exposed to the vapours and oxygen leakage in the system. The average uniform corrosion penetration rate was calculated by the weight change. To distinguish the types of corrosion cases, a piece of uncoated metal was used as a “sacrificial metal” to react with oxygen that enters the vessel during the immersion test, or to react with the residual oxygen trapped inside the immersion vessel. Then since a fixed amount of oxygen reacts with more metal surfaces in the same period of time, a weight increase would stop when all residual oxygen is consumed. This confirmed that the sealing mechanism functioned properly.

5.2.3 Corrosion Experimental Results

(i) Coating 1 (YSZ Zirconia, ZrO_2 8%Y_2O_3)

The first test was conducted for 5 h on coating #1. Figure 14 illustrates the condition of the specimen before and after the test. After immersion for 5 h in CuCl and post-immersion cleaning, the specimen displayed a green color which indicated copper deposits. The color became prominent once the sample was rinsed and cleaned with saturated EDTA. Copper deposits could also be seen by EDX images. However, a thin layer of YSZ on the base metal and a layer of copper (chloride) deposits were also attached on the base metal. The composition list from EDX results showed copper, indicating severe corrosion occurred and copper diffused through the coating. This may have arisen because the coating did not have sufficient thickness to resist the molten CuCl attack. The first coating of YSZ applied directly onto the base metal did not survive 5 h of exposure to molten CuCl. However, when the ceramic coating (YSZ) was applied to the base metal with a bond metal coating, it survived the immersion tests, but showed corrosion and erosion within its layers.

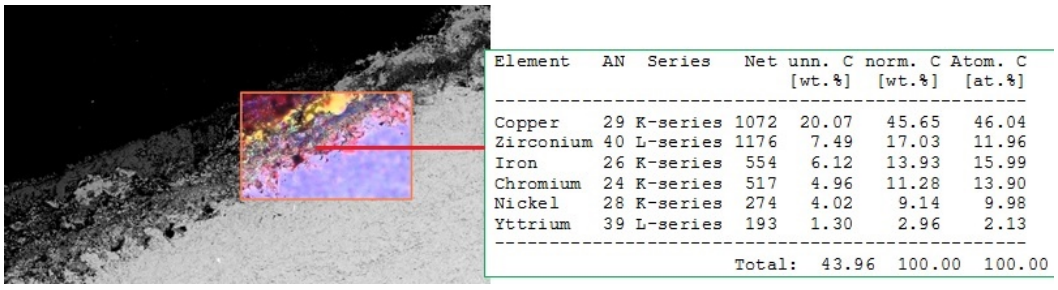

Element	AN	Series	Net unn. C [wt.%]	norm. C [wt.%]	Atom. C [at.%]
Copper	29	K-series	1072 20.07	45.65	46.04
Zirconium	40	L-series	1176 7.49	17.03	11.96
Iron	26	K-series	554 6.12	13.93	15.99
Chromium	24	K-series	517 4.96	11.28	13.90
Nickel	28	K-series	274 4.02	9.14	9.98
Yttrium	39	L-series	193 1.30	2.96	2.13
		Total:	43.96	100.00	100.00

Figure 14: SEM/EDX images of sample #1

(ii) Coating 2 (Diamalloy 4006 + YSZ)

A second test was performed on coating #2 for 48 h. The coating combination was more corrosion resistant in the molten CuCl solution (Fig. 15). After the 48 h test, the YSZ layer of coating was delaminated in some regions, as shown in Figure 4. In addition, SEM and EDX tests were conducted to evaluate the depth and severity of corrosion.

Some possible causes of the coating de-bonding may be differences between the thermal expansion coefficient of the coating and sample, or stress or attack from the molten CuCl. The coating remained intact

and there were no cracks or corrosions on the coated specimens. If the coating cracks, it could provide a pathway for the corrosive material to pass under the coating layer and react with the base metal.

Spectrum: Point

Element	AN	Series	Net unn. C [wt.%]	norm. C [wt.%]	Atom. C [at.%]
Iron	26	K-series	22335	88.29	89.90	71.09
Carbon	6	K-series	745	7.10	7.23	26.57
Manganese	25	K-series	562	1.64	1.67	1.34
Copper	29	K-series	107	0.91	0.93	0.65
Chlorine	17	K-series	230	0.28	0.28	0.35
		Total:		98.21	100.00	100.00

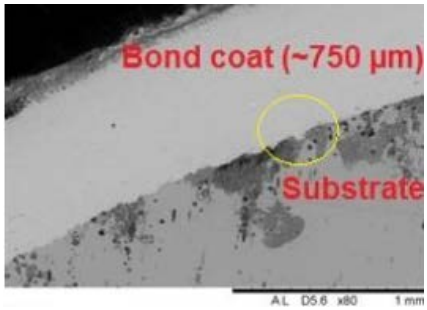

Figure 15: Bond coat and substrate interface images of sample #2

(iii) Coating 3 (Diamalloy 4006 - HVOF)

High velocity oxy-fuel coating spraying (HVOF) is a thermal spray coating technique in which melted material is sprayed onto a substrate at high temperature with a specified velocity. Using this technique with Diamalloy 4006 produced the most promising results as the coating survived exposure to molten CuCl.

Figure 16: Sample #3 before and after immersion tests

Figures 16 to 18 illustrate the sample, before and after immersion tests, SEM and EDX images of the sample, respectively. Additional coatings were tested. Diamalloy 4006 with an Al_2O_3 top survived for 40 h. An SHS coating combination failed to survive for 100 h. Molten CuCl was splitting in some cases to form copper deposits on the sample. It was also found that Diamalloy coatings performed much better than SHS-9172. Overall, Diamalloy 4006 (HVOF) proved best in the group of tests conducted although the sample tip was damaged. Alloys under consideration for future testing include: Hastelloy, Quartz Glass coating (if possible), Udimet 500, IN718, nickel-based superalloy Nimonic105; and any potential corrosion resistant alloy.

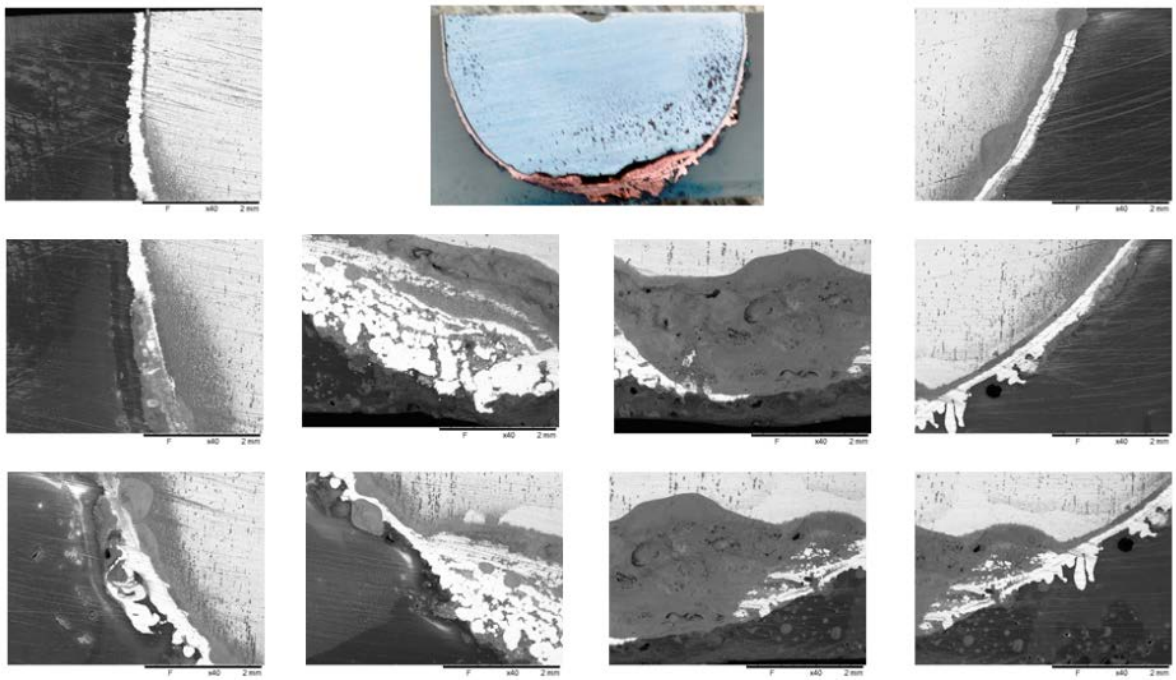

Figure 17: Scanning electron microscopy (SEM) images of sample #3

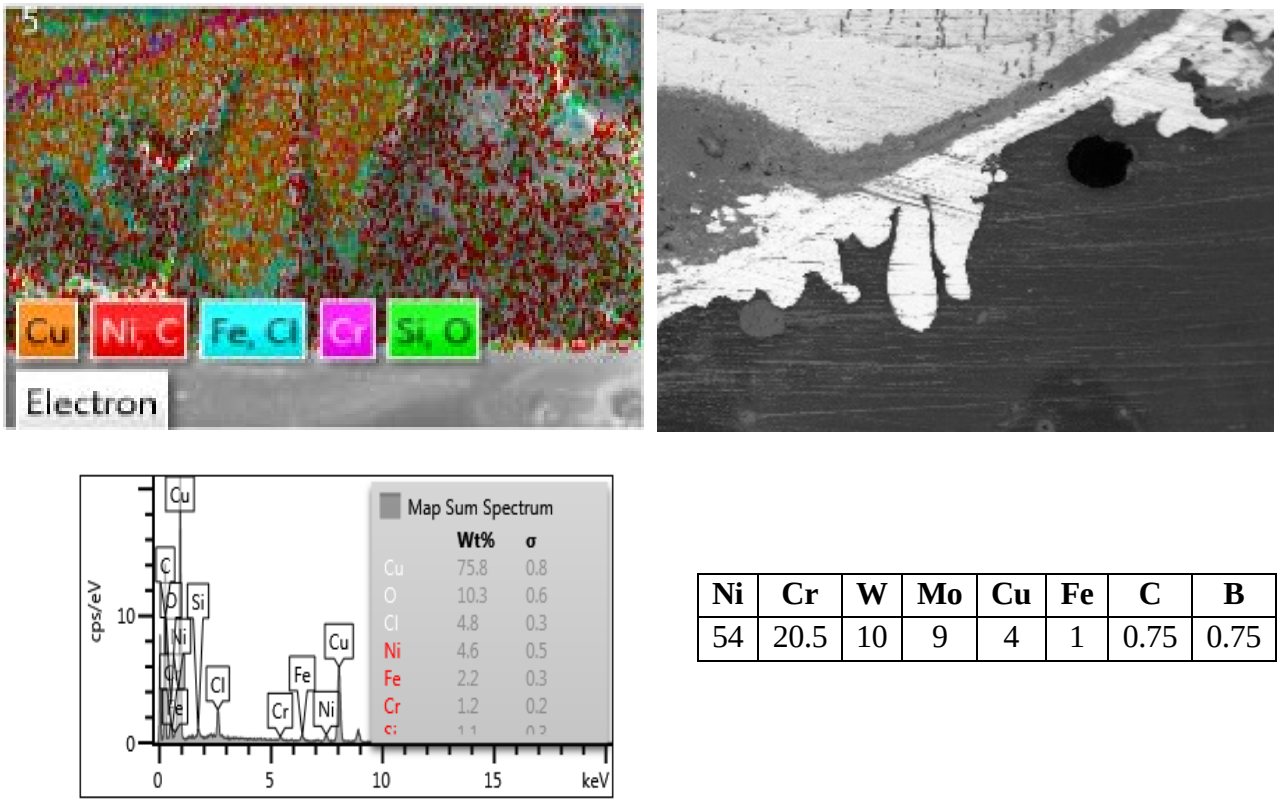

Ni	Cr	W	Mo	Cu	Fe	C	B
54	20.5	10	9	4	1	0.75	0.75

Figure 18: Energy dissipative X-ray spectroscopy (EDX) images of sample #3

6. System Integration

6.1 Integration of Lab-Scale Unit Operations

A team of researchers at UOIT has reported numerous advances in the integration of experimental lab-scale unit operations of the Cu-Cl cycle in the Clean Energy Research Laboratory (CERL) [50]. This includes integration of the electrolysis / hydrolysis, thermolysis / hydrolysis, and transport systems between the unit operations. A low-temperature test loop was developed to integrate the electrolysis (anolyte loop), crystallization cell and dissolution cell. A new dilution and precipitation cell has been integrated to lower the HCl concentration in the flow stream to hydrolysis. Also, a method to recover CuCl escaped from the crystallization cell has been demonstrated.

For linkage of electrolysis and hydrolysis steps, aqueous $CuCl_2$ is to be flash boiled into steam as it enters the hydrolysis reactor. The solution is pressurized to 2 MPa and heated to 200^oC. Heating is accomplished via heating tape wrapped around the inlet pipe to the hydrolysis reactor. The pre-boiling is performed to accelerate the hydrolysis reaction by increasing the thermal energy of reactants. Due to the constant flow required by integration of the processes, a new hydrolysis reactor has been designed. The new reactor design involves short pulses of fluid injection, allowing particles to settle out between pulses. Previous designs involving a cyclone separator were infeasible due to pulsating flow so an airlock system was selected instead. A rotary airlock at the bottom of the reactor allows for removal of $CuOCuCl_2$ salt. A heated “Clamshell” furnace allows for heating of steam within the reactor, in addition to heating the walls. The heated steam environment maximizes the rate of heat transfer. Then the solid powder of $CuOCuCl_2$ salt is extracted at a temperature of 400^oC and passed to the thermolysis reactor via screw conveyors. A schematic of the experimental layout is illustrated in Fig. 19.

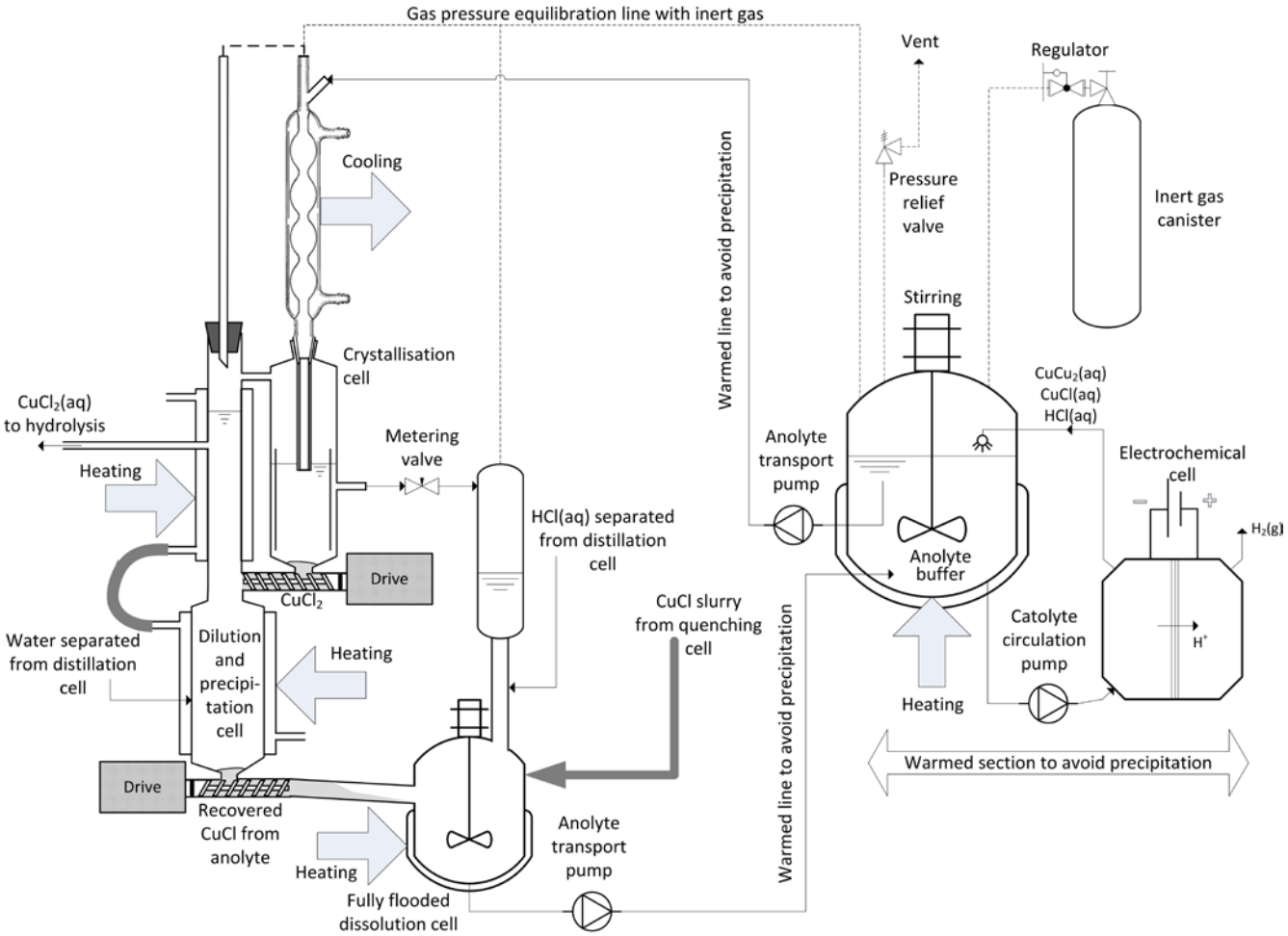

Figure 19: Proposed layout of the integrated unit operations of the Cu-Cl cycle at UOIT

For linkage of the hydrolysis and thermolysis reactors, as solid particles leave the hydrolysis reactor, a cooling step is necessary before they can be transported. Materials that can withstand exposure to $CuOCuCl_2$ and other corrosive materials are not heat resistant so the particles must be cooled. This is a challenging step to efficiently exchange heat from solids to a liquid. A flexible screw conveyor was used to convey the $CuOCuCl_2$ from the hydrolysis step to the oxygen reactor. The selection for the screw conveyor was based on 3 factors: temperature resistance, corrosion resistance, and flow rate. The screw conveyor is operated on a duty cycle to allow the heat exchanger time to cool down the particles. The thermolysis reactor consists of an overflow vessel which melts the input of $CuOCuCl_2$ and overflows the output of liquid CuCl while venting oxygen gas to a fume hood. A current challenge with this reactor is to find a way to purge the system with an inert gas to prevent oxidation of the CuCl that is produced, as well as purging the quench

tube. A hydraulic tilt mechanism has been developed to allow a safe shutdown procedure of the oxygen reactor and purge liquid CuCl from the system. The tilt control will also allow for the control of flow rates into the quench, working in tandem with the conveyor to allow more accurate flow control.

The integration phase between the oxygen reactor and dissolution cells leads to the CuCl/HCl electrolyser. The slurry pump for CuCl transport must handle high temperature and highly corrosive solids. Three options are available for cooled CuCl to be transported to the dissolution cells (as dry solids or wet slurry). Two designs involve dry solids, whereas another delivers a required flowrate of water-CuCl slurry.

In the first option, water-CuCl is removed from the quench tank and the slurry is pumped to the dissolution cell. A vibrating sieve collects the slurry and delivers CuCl solids to the dissolution cell. Then a pump recycles the separated water into the quench cell. The stoichiometric input for this integration phase to yield 0.1 kg of hydrogen per day requires a transported rate of CuCl from the oxygen reactor of approximately 0.4125 kg/h. To optimize the amount of thermal energy transferred into the quench, the overflowed CuCl is dropped down a tube for heat recovery. The heat recovery allows for a much smaller quench bath vessel and easier integration. However, a significant difficulty is the possibility of oxidation of the falling CuCl. The process is completely purged with an inert gas.

In the second option, water-CuCl coming from the quench tank flows to a sifter. Water is then pumped back to the quench tank. The CuCl solids are placed on a conveyer and transported to the dissolution cell.

Thirdly, the water-CuCl slurry can instead be taken from the quench tank, at a desired concentration, by measuring the mass of collected CuCl. Then the slurry is pumped to the dissolution cell. This option assumes that water is pumped back to quench tank from the hydrolysis reactor. In terms of energy utilization, this option is the most efficient approach. Of the three approaches considered, the slurry pump is the core component system integration since it establishes transport at the desired concentration of water-CuCl that is required at the dissolution cell. Accurate knowledge of the ratios of CuCl to $CuCl_2$ is critical to allow for an efficient system to extract the $CuCl_2$, which is then fed to the hydrolysis reactor.

6.2 Intermediate Heat Exchanger for SCWR

The Canadian SuperCritical Water-cooled Reactor (SCWR) is a Generation IV concept of a future nuclear plan designed to operate at pressures of 25 MPa with reactor outlet temperatures up to 625ºC. These operating conditions make it a suitable candidate for hydrogen cogeneration with the thermochemical Cu-Cl cycle. Recent studies [49] have conducted an analysis of the intermediate heat exchanger linking a SCWR and Cu-Cl cycle. The Canadian SCWR concept consists of 336 fuel channels, with each channel housing a 5 m long fuel assembly. The core uses a pressurized inlet plenum that is connected to a low-pressure calandria vessel. The calandria vessel contains a heavy water moderator that will surround the 336 fuel channels. Each of the fuel channels contains a fuel assembly that features a central flow tube and two-ring-fuel-element configuration. The fuel assembly was designed with a two-pass counter-flow configuration, where the coolant travels downward through the central tube and then flows upwards through the fuel elements.

In the case of a no-reheat cycle, there are three potential points of heat extraction that have been studied (Fig. 20). The ideal heat extraction location would be the reactor outlet since its temperature is approximately 625^{o}C; this point is circled in the figure. At the other two points, additional sources of heat would be required with the SCWR process heat.

For a counter-flow double-pipe heat exchanger, the hot and cold fluids will enter the heat exchanger from opposite ends. The hot fluid is the SCW reactor coolant which would flow through the inner pipe. The cold fluid is a separate SCW working fluid flowing through the annulus gap of the heat exchanger. The operating parameters are presented in Table 4. While the 4-stage Cu-Cl cycle only has a maximum temperature requirement of 530^{o}C, the outlet temperature of the SCW working fluid was set at 600^{o}C. In the event of a leak in the inner pipe, the SCW working fluid would flow into the inner pipe, thus containing the SCW reactor coolant. Pipe diameters and thicknesses were selected according to ASME standards. As per ASME standards, the design stress of a pressure boundary component is less than a third of the Ultimate Tensile Strength (UTS) of the material. Along with the parameters described in Table 4, the percentage of reactor thermal power to be diverted was set to 10% for a reference case.

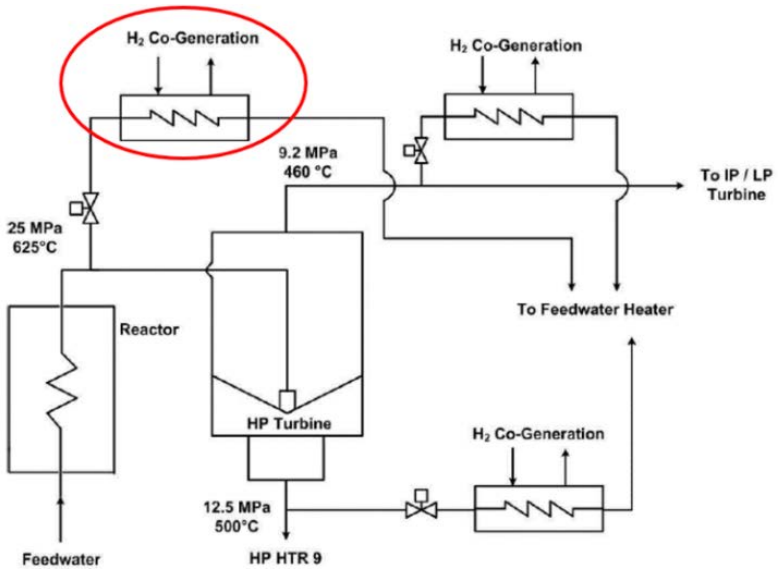

Figure 20: Heat extraction points for linkage of the SCWR and Cu-Cl cycle

Operating Parameter	**Inner Pipe (Hot Side)**	**Annulus Gap (Cold Side)**
Fluid	SCW reactor coolant	SCW Working Fluid
Pressure (MPa)	25	25.5
Inlet temperature (°C)	625	350
Outlet temperature (°C)	350	600
Mass flux (kg/m^2·s)	1500	1500
Inner diameter (mm)	20.9	32.5
Outer diameter (mm)	26.7	42.2
Pipe thickness (mm)	2.87	5.80

Table 4: Operating parameters for reference heat exchanger

The reference case used operating pressures of 25 MPa and 25.5 MPa for the hot and cold side, respectively. A mass flux of 1500 kg/m^2·s was used for both the hot side and cold side. To achieve the desired heat transfer to the SCW working fluid on the cold side, a total of 256 pipes with a length of 44.6 m per pipe would be needed. Figure 21 also demonstrates that at approximately 30 m from the hot side inlet, the temperature profile begins to flatten out. At this point, it is also evident that fluids begin to enter a pseudocritical region. This is shown by the variation in heat transfer coefficient (HTC) profiles after this point. This variation is expected in the pseudocritical region. Figure 21 also shows rounded peaks in the

HTC profile for both the hot side and cold side due to the location of pseudocritical points from the hot side inlet. To remove these variations, the inlet temperature of the cold side and the outlet temperature of the hot side would need to be adjusted. This would keep the operating point of the heat exchanger above the pseudocritical point, thus removing the pseuodocritical region.

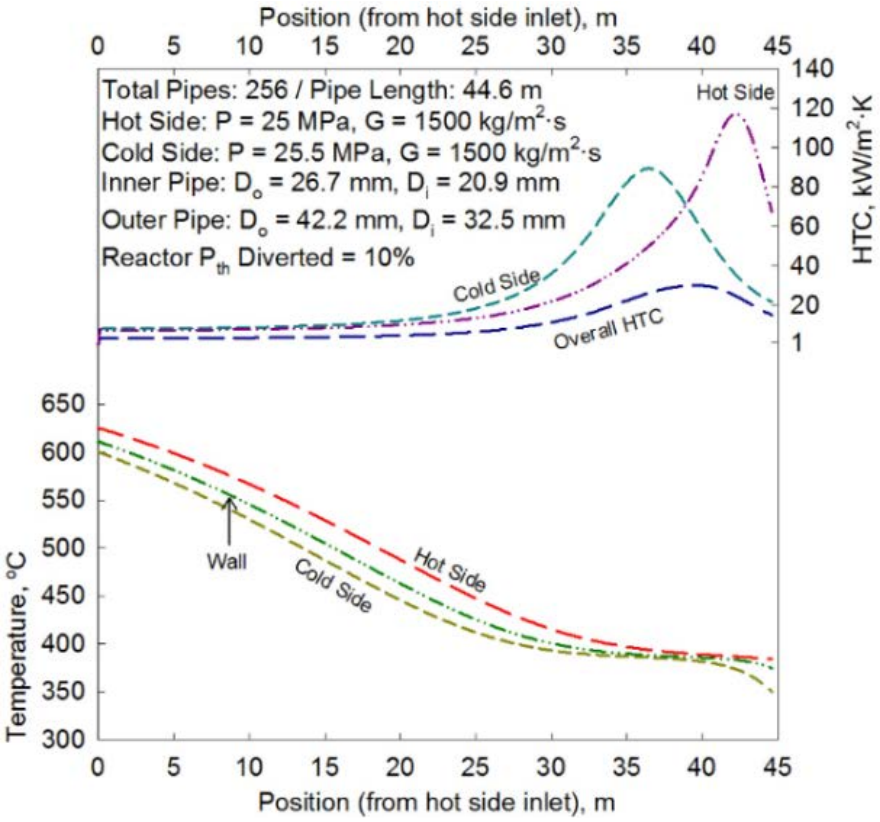

Figure 21: Heat transfer coefficient temperature profiles for reference case

Depending on the selected production rate, thermal energy requirements of the Cu-Cl cycle may change. As a result, it is important to consider how a different thermal energy requirement will impact the overall size of the heat exchanger. Increasing the amount of energy being diverted from a SCW to a Cu-Cl cycle also increases the size of the heat exchanger.

6.3 Cascaded Heat Pumps for Solar Thermochemical Cu-Cl Cycle

Upgrading heat from nuclear power plants or other industrial waste heat sources up to higher temperatures needed by the Cu-Cl cycle can be achieved through chemical pumps [51-53]. Zamfirescu et al. [51] developed a CuCl vapor compression heat pump to meet the highest temperature requirement in the

Cu_2OCl_2 decomposition reactor (500-530^oC). The CuCl heat pump requires a bottom heat pump cascaded with it, since its evaporator operates at significantly sub-atmospheric pressure (0.2 mbar) to accommodate source temperatures greater than 480^oC and to achieve an evaporator temperature of 300^oC. Akmahdi [54] developed a cascaded heat pump consisting of a CuCl vapor compression heat pump and a bottom heat pump to upgrade heat from about a 300^oC source temperature to the required temperature of the copper oxychloride decomposition reactor of 500-530 ^oC.

The cascaded copper (I) chloride – biphenyl heat pump CuCl-$(C_6H_5)_2$ is shown in Fig. 22. The bottom heat pump operates with biphenyl as a working fluid. A two-phase mixed biphenyl at state 25 gains heat as it flows through the heat exchanger, recovering heat from the low temperature heat source and exits as a saturated liquid at state 26. Prior to compression, the saturated liquid at state 26 is superheated further by an internal heat recovery heat exchanger HX6. The heat is recovered from the stream at state 23, which then exits the heat exchanger HX5 which is responsible for evaporating the CuCl in the CuCl heat pump evaporator. The heat exchanger HX6 is necessary due to the retrograde nature of the biphenyl. If the saturated vapor is pressurized in the compressor, it becomes a two-phase vapor-liquid fluid that eventually damages the compressor. However, preheating the biphenyl will assure that it remains a vapor during compression. The superheated biphenyl leaves HX6 at state 27 and is compressed by compressor C4 to state 22 which is used to evaporate the CuCl through heat exchanger HX5. Almahdi [54] analysed the temperature, pressure, and mole flow rate of the state points calculated from Aspen Plus. The thermodynamic properties such as molar enthalpy and molar entropy were presented over a range of operating conditions [54].

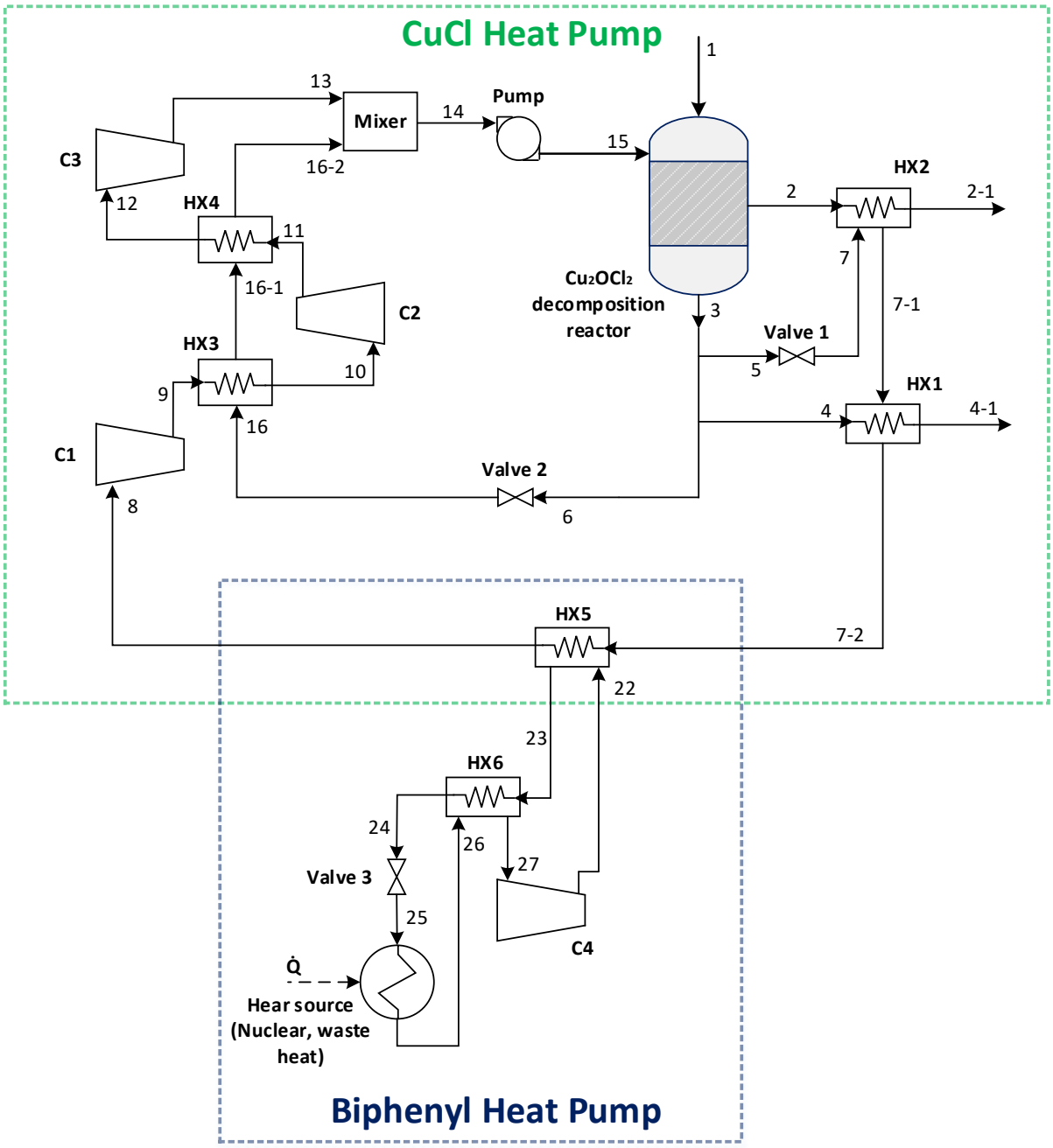

Figure 22: Schematic of Copper (I) Chloride – Biphenyl Cascaded Heat Pump (CuCl-$(C_6H_5)_2$)

In Fig. 22, at the lowest pressure of 0.1 bar, the CuCl-biphenyl cascaded heat pump has a lower overall energetic COP (0.52) than the sole biphenyl heat pump (0.85). Its exergetic COP (0.62), however, is greater compared to the exergetic COP (0.52) of the single heat pump. In contrast to the improvement in the CuCl heat pump with the increase of its evaporator pressure, the bottom biphenyl heat pump cycle will experience a reduction in its energetic and exergetic COPs. As the evaporator pressure of the CuCl heat

pump (stream 7 to 8) increases, high temperature working fluids in the bottom cycle condenser will be expected to evaporate the fluids in the top cycle evaporator. That high temperature source should be provided by the bottom biphenyl heat pump to the CuCl heat pump evaporator which cannot be obtained unless the biphenyl heat sink pressure is raised. This would eventually yield more power consumption and cause COPs to decrease. The CuCl-biphenyl cascaded heat pump will have a similar drop in energetic and exergetic COPs for the same reason.

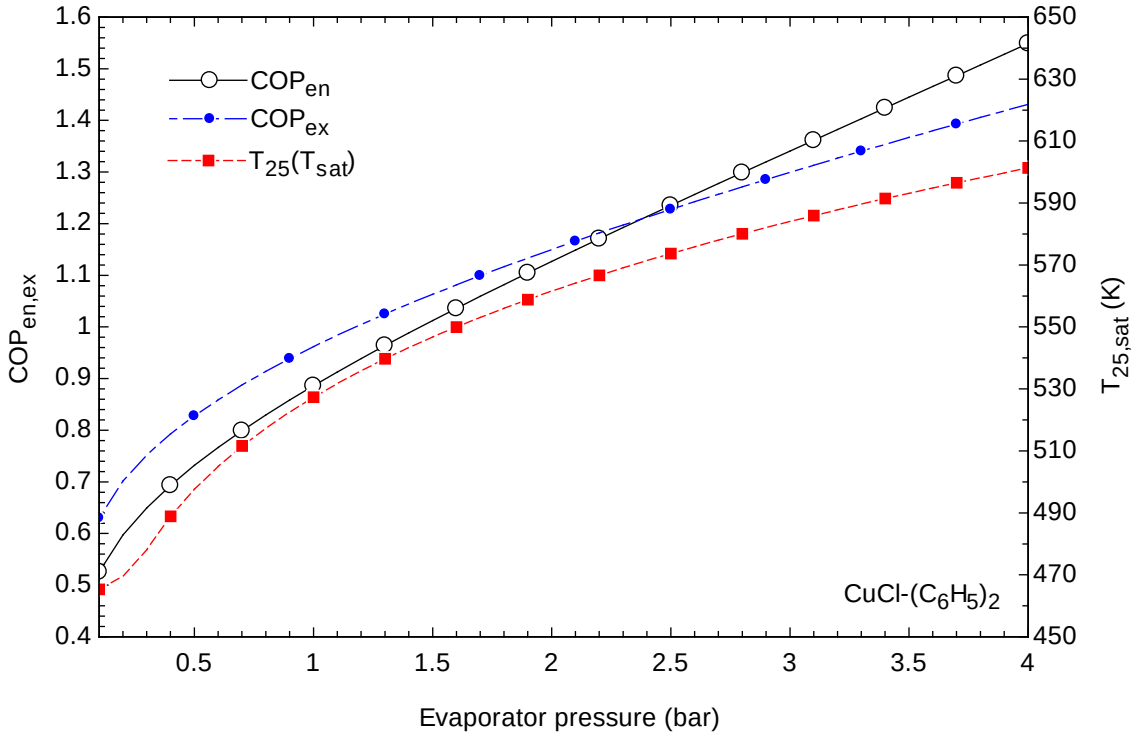

Figure 23: Variation of COPs of CuCl-biphenyl cascaded heat pump with biphenyl evaporator pressure

6.4 Solar Thermochemical Cu-Cl Cycle

In addition to nuclear energy as a potential heat source for the Cu-Cl cycle, another viable source investigated was solar energy [49]. A process flow diagram for a solar hydrogen plant is illustrated in Fig. 1, including a central receiver, molten salt transport, endothermic Cu-Cl reactions and a Rankine cycle. The central receiver is a parabolic concentrated solar collector that uses a field of heliostat mirrors to focus a large area of energy onto a smaller receiver surface area, resulting in a concentrated radiation input. There

are two forms of solar radiation input – beam radiation (or direct normal irradiation) and diffuse radiation. Beam radiation was used for the central receiver of the concentrated solar energy system.

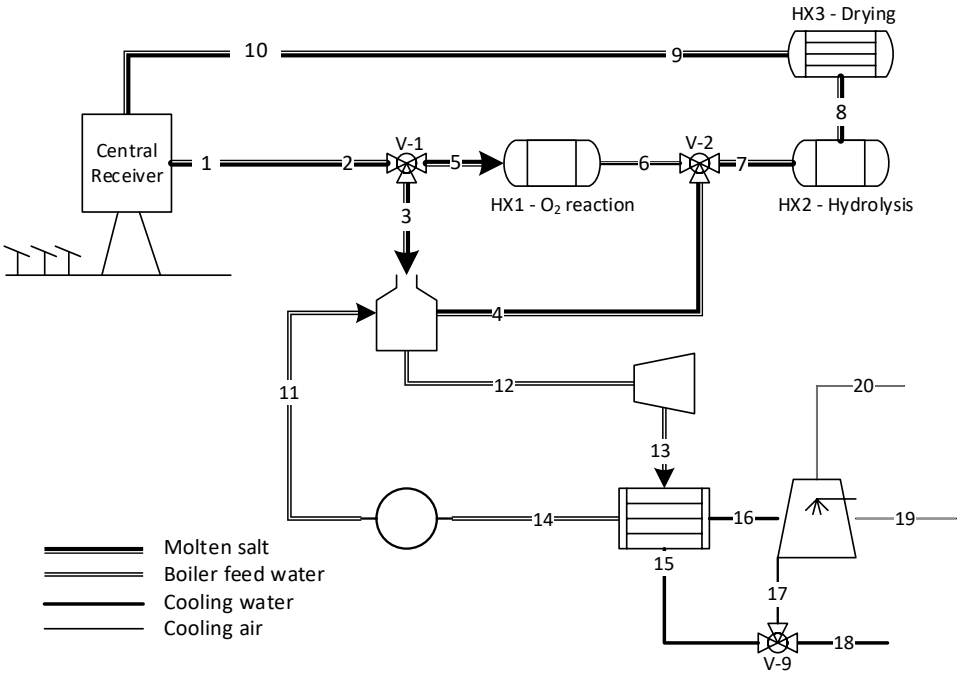

Figure 22: Process flow diagram for a solar based copper-chlorine cycle

There are two types of losses from the central receiver system: heliostat field losses and receiver losses. The heliostat field losses consist of shadowing, blocking, reflectance and atmospheric attenuation which are related to optical radiation losses. The receiver losses consist of optical radiation losses such as spillage and absorptance as well as thermal losses such as conduction, convection and radiation losses. Table 5 summarizes the parameters used and calculated for a case study of a solar based Cu-Cl plant. The estimated hydrogen production rate and production efficiency for a solar Cu-Cl plant are 0.89 kg H_2/s and 20%, respectively. The total energy input to the solar plant is 785 MW but only 309 MW is absorbed by the molten salt resulting in a central receiver efficiency of 49%. The Rankine cycle efficiency associated with the electrical energy input for the hydrogen production step is about 26%. To simulate the hydrogen plant output accurately, the monthly variations in solar energy input were taken into account. Irradiation values were converted to irradiance by dividing by the daily average hours of daylight for each month taken from the Canadian Weather and Energy Engineering Data Set (CWEEDS).

Parameters	Value
Solar irradiance (constant, uninterrupted), I	0.8 kW/m^2
Heliostat field diameter, D_{field}	1,000 m
Air temperature, T_a	298 K
Air pressure, P_a	0.101 MPa
Wind speed, V_a	1 m/s
Pipe length, L_{pi}	300 m
Turbine inlet temperature, T_{12}	673 K
Turbine inlet pressure, P_{12}	2 MPa
Condenser pressure, P_{13}	0.01 MPa
Cooling water temperature, T_{15}	293 K
Total available solar energy input rate, IA_{field}	785 MW
Total energy rate absorbed by molten salt, $\dot{Q}_{ab}$	309 MW
Estimated hydrogen production rate, $\dot{m}_{H_2}$	0.89 kg/s
Central receiver efficiency, η_{re}	0.49
Thermal efficiency of Rankine cycle, η_{th}	0.26
Production efficiency (H_2 HHV), η_{pr}	0.20

Table 5: Design parameters for solar hydrogen plant case study

7. Conclusions

This paper presented an overview of recent advances in the development and scale-up of the thermochemical Cu-Cl cycle of hydrogen production. It extends previous reports [2-5, 16, 25] by a Canadian-led international team, including a number of institutions from Canada, U.S., China, Slovenia and Romania. Recent progress was presented for electrochemical cell analysis, membrane characterization, constituent solubility and metastability in ternary mixtures, crystallization measurements, materials corrosion, surface coating performance, system integration, scale-up of unit operations, cascaded heat pumps for heat upgrading, and linkage with solar and nuclear plants. The team's next future goal is an intermediate step of system integration of lab-scale unit operations, followed by a medium term goal of scale-up of the integrated Cu-Cl cycle to a small pilot plant. Ultimately the long term goal is a commercial hydrogen plant in connection with Canada's Generation IV reactor, SCWR (Super-Critical Water Reactor), as part of the Generation IV International Forum (GIF) for hydrogen production with the next generation of nuclear reactors.

Acknowledgements

Support of this research from Canadian Nuclear Laboratories, Ontario Research Excellence Fund and the Natural Sciences and Engineering Research Council of Canada are gratefully acknowledged.

References

[1] Lewis, M. A., Serban, M., Basco, J. K., "Hydrogen Production at <550C Using a Low Temperature Thermochemical Cycle", ANS/ENS Exposition, New Orleans, Nov. 2003

[2] Naterer, G. F., Suppiah, S., Stolberg, L., Lewis, M., Wang, Z., Rosen, M. A., Dincer, I., Gabriel, K., Odukoya, A., Secnik, E., Easton, E. B., Papangelakis, V., "Progress in Thermochemical Hydrogen Production with the Copper-Chlorine Cycle", International Journal of Hydrogen Energy, vol. 40, no. 19, pp. 6283 – 6295, May, 2015

[3] Naterer, G. F., Suppiah, S., Stolberg, L., Lewis, M., Ferrandon, M., Wang, W., Dincer, I., Gabriel, K., Rosen, M. A., Secnik, E., Easton, E. B., Trevani, L., Pioro, I., Tremaine, P., Lvov, S., Jiang, J., Rizvi, G., Ikeda, B. M., Lu, L., Kaye, M., Smith W. R., Mostaghimi, J., Spekkens, P., Fowler, M., Avsec, J., "Clean Hydrogen Production with the Cu-Cl Cycle – Progress of International Consortium, I: Experimental Unit Operations", International Journal of Hydrogen Energy, vol. 36, pp. 15472 – 15485, 2011

[4] Naterer, G. F., Suppiah, S., Stolberg, L., Lewis, M., Ferrandon, M., Wang, W., Dincer, I., Gabriel, K., Rosen, M. A., Secnik, E., Easton, E. B., Trevani, L., Pioro, I., Tremaine, P., Lvov, S., Jiang, J., Rizvi, G., Ikeda, B. M., Lu, L., Kaye, M., Smith, W. R., Mostaghimi, J., Spekkens, P., Fowler, M., Avsec, J., "Clean Hydrogen Production with the Cu-Cl Cycle – Progress of International Consortium, II: Simulations, Thermochemical Data and Materials", International Journal of Hydrogen Energy, vol. 36, pp. 15486 – 15501, 2011

[5] Rosen, M. A., Naterer, G. F., Chukwu, C. C., Sadhankar, R., Suppiah, S., “Nuclear-based Hydrogen Production with a Thermochemical Copper-Chlorine Cycle and Supercritical Water Reactor: Equipment Scale-up and Process Simulation”, International Journal of Energy Research, vol. 36, no. 4, pp. 456 – 465, 2012

[6] Lewis, M., Taylor, A., "High Temperature Thermochemical Processes", DOE Hydrogen Program, Annual Progress Report, Washington DC, pp. 182 – 185, 2006

[7] Kasahara, S., Kubo, S., Hino, R., Onuki, K., Nomura, M., Nakao, S., "Flow Sheet Study of the Thermochemical Tater-splitting Iodine–Sulfur Process for Effective Hydrogen Production", International Journal of Hydrogen Energy, vol. 32, no. 4, pp. 489 – 496, 2007

[8] Carty, R. H., Mazumder, M., Schreider, J. D., Panborn, J. B., "Thermochemical Hydrogen Production", Gas Research Institute for the Institute of Gas Technology, GRI Report 80-0023, vol. 1, Chicago, IL 60616, 1981

[9] Knoche, K. F., Schuster, P., Ritterbex, T., "Thermochemical Production of Hydrogen by a Vanadium / Chlorine cycle. II: Experimental Investigation of the Individual Reactions", International Journal of Hydrogen Energy, vol. 9, pp. 473 – 482, 1984

[10] Funk, J. E., "Thermochemical Hydrogen Production: Past and Present", International Journal of Hydrogen Energy, vol. 26, no. 3, pp. 185 – 190, 2001

[11] Naterer, G. F., Dincer, I, Zamfirescu, C., Hydrogen Production from Nuclear Energy (492 pages), Springer, New York, NY, 2013

[12] Stolberg, L., Electrolysis Cell for the Conversion of Cuprous Chloride in Hydrochloric Acid to Cupric Chloride and Hydrogen Gas, U.S. Patent No. 0051469; 2010

[13] Kettner, A., Stolberg, L., Li, H., Shkarupin, A., Suppiah, S., Electrolysis Cell with Multiple Membranes for CuCl/HCl Electrolysis in Hydrogen Production, Patent Pending, PCT/CA2013/000294, 2013

[14] Balashov, V. N., Schatz, R. S., Chalkova, E., Akinfiev, N. N., Fedkin, M. V., Lvov, S., "CuCl Electrolysis for Hydrogen Production in the Cu–Cl Thermochemical Cycle", Journal of The Electrochemical Society, vol. 158, no. 3, pp. B266-B275, 2011

[15] Ranganathan, S., Easton, E. B., "High Performance Ceramic Carbon Electrode-based Anodes for Use in the Cu–Cl Thermochemical Cycle for Hydrogen Production", International Journal of Hydrogen Energy, vol. 35, no. 3, pp. 1001-1007, 2010

[16] Naterer, G. F., Suppiah, S., Stolberg, L., Lewis, M., Wang, Z., Dincer, I., Rosen, M. A., Gabriel, K., Secnik, E., Easton, E. B., Pioro, I., Lvov, S., Jiang, J., Mostaghimi, J., Ikeda, B. M., Rizvi, G., Lu, L., Odukoya, A., Spekkens, P., Fowler, M., Avsec, J., “Progress of International Hydrogen Production Network for the Thermochemical Cu-Cl Cycle”, International Journal of Hydrogen Energy, vol. 38, pp. 740 – 759, January 2013

[17] Lewis, M. A., Ahmed, S., Lvov, S., Fan, C., "Membrane/Electrolyzer Development in the Cu-Cl Thermochemical Cycle", FY 2012 annual report, DOE Hydrogen and Fuel Cells Program, 2012

[18] Edge, P. S. R., Easton, E. B., "Comparison of Novel Anode Materials for the Production of Hydrogen Using CuCl/HCl Electrolyzers", ECS Transactions, vol. 53, no. 9, p. 11-20, 2013

[19] Wang Z., Daggupati V. N., Marin G., Pope K., Xiong Y., Secnik E., Naterer G. F., Gabriel K. S., "Towards Integration of Hydrolysis, Decomposition and Electrolysis Processes of the Cu-Cl Thermochemical Water Splitting Cycle", International Journal of Hydrogen Energy, vol. 37, pp. 16557-16569, 2012

[20] Leray J. L., "Growth Kinetics of Hydrated Cupric Chloride", Journal of Crystal Growth, vol. 3, pp. 344-349, 1968

[21] Abdel Basir, S. M., "Recovery of Cupric Chloride from Spent Copper Etchant Solution: A Mechanistic Study", Hydrometallurgy, vol. 69, pp. 135-143, 2003

[22] Cakir, O., "Copper Etching with Cupric Chloride and Regeneration of Waste Etchant", Journal of Materials Processing Technology, vol. 175, pp. 63–68, 2006

[23] Yang, Z., Huang, C., Ji, X., Wang, Y., "New Electrolytic Method for On-Site Regeneration of Acidic Copper (II) Chloride Etchant in Printed Circuit Board Production", International Journal of Electrochemical Sciece, vol. 8, pp. 6258 – 6268, 2013

[24] Ghandehariun, S., Rosen, M.A., Naterer, G.F., Wang, Z., "Pinch analysis for recycling thermal energy in the Cu-Cl cycle", International Journal of Hydrogen Energy, vol. 37, pp. 16535-16541, 2012

[25] Naterer, G.F., Suppiah, S., Stolberg, L., Lewis, M., Ahmed, S., Wang, Z., Rosen, M.A., Dincer, I., Gabriel, K., Secnik, E., Easton, E.B., Lvov, S.N., Papangelakis, V., Odukoya, A., "Progress of international program on hydrogen production with the copper-chlorine cycle", International Journal of Hydrogen Energy, vol. 39, pp. 2431-2445, 2014

[26] O'Connor, J. J., Thomasian, A., Armington, A. F., "Analysis and Solubility of Cuprous Chloride in Hydrochloric Acid Solutions", Journal of Electrochemical Society: Electrochemical Science, pp. 931-932, Sept. 1968

[27] Fritz, J. "Solubility of Cuprous Chloride in Various Soluble Aqueous Chlorides", Journal of Chemical Engineering Data, vol. 27, pp. 188-193, 1982

[28] Ferrandon, M.S., Lewis, M. A., Tatterson, D. F., Gross, A., Doizi, D., Croize, L., Dauvois, V., Roujou, J. L., Zanella, Y., Carles, P., "Hydrogen Production by the Cu–Cl Thermochemical Cycle: Investigation of

the Key Step of Hydrolysing $CuCl_2$ to Cu_2OCl_2 and HCl using a Spray Reactor", International Journal of Hydrogen Energy, vol. 35, no. 3, pp. 992-1000, 2010

[29] Naterer, G.F., Suppiah, S., Lewis, M. A., Gabriel, K. S., Dincer, I., Rosen, M. A., Fowler, M., Rizvi, G., Easton, E. B., Ikeda, B. M., "Recent Canadian Advances in Nuclear-Based Hydrogen Production and the Thermochemical Cu–Cl Cycle." International Journal of Hydrogen Energy, vol. 34, no. 7, pp. 2901-2917, 2009

[30] Pope, K., Naterer, G. F., Wang, Z. L., "Nitrogen Carrier Gas Flow for Reduced Steam Requirements of Water Splitting in a Packed Bed Hydrolysis Reactor", Experimental Thermal and Fluid Science, vol. 44, pp. 815-824, 2013

[31] Daggupati, V., Naterer, G. F., Gabriel, K., Gravelsins, R., Wang, Z., “Equilibrium Conversion in Cu-Cl Cycle Multiphase Processes of Hydrogen Production”, Thermochimica Acta, vol. 496, pp. 117 – 123, December 2009

[32] Zamfirescu, C., Dincer, I., Naterer, G. F., “Thermophysical Properties of Copper Compounds in Copper-Chlorine Thermochemical Water Splitting Cycles”, International Journal of Hydrogen Energy, vol. 35, pp. 4839 – 4852, May 2010

[33] Xie, J., Wang, X., Li, A., Li, F., Zhou, Y., "Corrosion Behaviour of Selected Mn+1AXn Phases in Hot Concentrated HCl solution: Effect on an Element and MX Layer", Corrosion Science, vol. 60, pp. 129-135, 2012

[34] Wu, D., Mao, F., Wang, S., Zhou, Z., "Low-temperature Fabrication Route for Enhancing Mechanical Properties and Corrosion Resistance of Porous Mullite Ceramics through Homogeneously Mullite Sol-coating Method", Ceramic Processing, vol. 14, pp. 677-681, 2013

[35] Sure, J., Shankar, A., Ramya, S., Mudali, U., "Molten Salt Corrosion of High Density Graphite and Partially Stabilized Zirconia Coated High Density Graphite in Molten LiCl-KCl Salt", Ceramics International, vol. 38, pp. 2803-2812, 2012

[36] Kamali, A. R., Fray, D. J. "Molten Salt Corrosion of Graphite as a Possible Way to Make Carbon Nanostructures", Carbon, vol. 56, pp. 121-131, 2013

[37] Vignarooban, K., Pugazhendi, P., Tucker, C., Gervasio, D., Kannan, A. "Corrosion Resistance of Hastelloys in Molten Metal-Chloride Heat-Transfer Fluids for Concentrating Solar Power Applications", Solar Energy, vol. 103, pp. 62-69, 2014

[38] Sellers, R., Cheng, W., Anderson, M., Sridharan, K., Wang, C., Allen, T., "Materials Corrosion in Molten LiF-NaF-KF Eutectic Salt Under Different Reduction-Oxidation Conditions", Proceedings of ICAPP. Paper 12189. Chicago: USA, 2012

[39] Siantar, E., "Study of the Effect of Molten CuCl Immersion Test on Alloys with High Ni-Content with and without Surface Coatings", Department of Automotive, Mechanical and Manufacturing Engineering, Master's Thesis, UOIT, Canada, 2012

[40] Orhan M. F., Dincer I., Rosen M. A., "Exergoeconomic Analysis of a Thermochemical Copper-chlorine Cycle for Hydrogen Production using Specific Exergy Cost (SPECO) Method", Thermochimica Acta, vol. 497, pp. 60-66, 2010

[41] Orhan M. F., Dincer I., Rosen M. A., "An Exergy-Cost-Energy-Mass Analysis of a Hybrid Copper-Chlorine Thermochemical Cycle for Hydrogen Production", International Journal of Hydrogen Energy, vol. 35, pp. 4831-4838, 2010

[42] Ozbilen A., Dincer I., Rosen M. A., "A Comparative Life Cycle Analysis of Hydrogen Production via Thermochemical Water Splitting Using a Cu-Cl Cycle", International Journal of Hydrogen Energy, vol. 36, pp. 11321-11327, 2011

[43] Ozbilen A., Dincer I., Rosen M. A., "Environmental Evaluation of Hydrogen Production via Thermochemical Water Splitting using the Cu-Cl Cycle: A Parametric Study", International Journal of Hydrogen Energy, vol. 36, pp. 9514-9528, 2011

[44] Haseli, Y., Naterer, G. F., Dincer, I., “Comparative Assessment of Greenhouse Gas Mitigation of Hydrogen Passenger Trains", International Journal of Hydrogen Energy, vol. 33, pp. 1788 – 1796, April 2008

[45] Balta M. T., Dincer I., Hepbasli A., "Exergoeconomic Analysis of a Hybrid Copper-Chlorine Cycle Driven by Geothermal Energy for Hydrogen Production", International Journal of Hydrogen Energy, vol. 36, pp. 11300-11308, 2011

[46] Ratlamwala T. A. H., I. Dincer. "Performance Assessment of Solar Based Integrated Cu-Cl Systems for Hydrogen Production", Solar Energy, vol. 95, pp. 345-356, 2013

[47] Wang, Z., G. F. Naterer, K. S. Gabriel, E. Secnik, R. Gravelsins, V. Daggupati, "Thermal Design of a Solar Hydrogen Plant with a Copper-Chlorine Cycle and Molten Salt Energy Storage", International Journal of Hydrogen Energy, vol. 36, pp. 11258-11272, 2011

[48] Orhan, M., Dincer, I., Naterer, G. F., Rosen, M. A., “Coupling of Copper-Chlorine Hybrid Thermochemical Water Splitting Cycle with a Desalination Plant for Hydrogen Production from Nuclear Energy”, International Journal of Hydrogen Energy, vol. 35, pp. 1560 – 1574, February 2010

[49] Suppiah, S., Naterer, G. F., Rosen, M. A., Wang, Z., et al., Clean Hydrogen Production with Water Splitting Technologies, ORF Workshop, Oshawa, Ontario, May 7, 2015

[50] Suppiah, S., Naterer, G. F., Rosen, M. A., Jianu, O., et al., Clean Hydrogen Production with Water Splitting Technologies, ORF Workshop, Oshawa, Ontario, June 20, 2016

[51] Zamfirescu, C., Naterer, G. F., Dincer, I., “Vapor Compression CuCl Heat Pump Integrated with a Thermochemical Water Splitting Plant”, Thermochimica Acta, vol. 512, pp. 40 – 48, 2011

[52] Zamfirescu, C., Naterer, G. F., Dincer, I., “Upgrading of Waste Heat for Combined Power and Hydrogen Production with Nuclear Reactors”, ASME Journal of Engineering for Gas Turbines and Power, vol. 132, no. 10, pp. 102911 – 102919, 2010

[53] Zamfirescu, C., Dincer, I., Naterer, G. F., “Performance Evaluation of Organic and Titanium Based Working Fluids for High Temperature Heat Pumps”, Thermochimica Acta, vol. 496, pp. 18 – 25, 2009

[54] Almahdi, M., “Integrated Heat Pump Options for Heat Upgrading in Cu-Cl Cycle for Hydrogen Production”, MASc Thesis, Department of Mechanical Engineering, UOIT, Oshawa, Ontario, 2016